

1 Peatlands and their carbon dynamics in northern high latitudes from 2 1990 to 2300: A process-based biogeochemistry model analysis

3 Bailu Zhao¹, Qianlai Zhuang^{1,2}

4 ¹ Department of Earth, Atmospheric, and Planetary Sciences, Purdue University, West Lafayette, IN 47907, USA

5 ² Department of Agronomy, Purdue University, West Lafayette, IN 47907, USA

6 *Correspondence to:* Qianlai Zhuang (qzhuang@purdue.edu)

7 **Abstract.** Northern peatlands ~~are a large C sink~~ have been a large C sink during the Holocene, but whether they will
8 keep being a C sink under future climate change is uncertain. This study simulates the responses of northern peatlands to
9 future climate until 2300 with a Peatland version Terrestrial Ecosystem Model (PTEM). The simulations are driven with two
10 sets of CMIP5 climate data (IPSL-CM5A-LR and bcc-csm1-1) under three warming scenarios (RCP2.6, 4.5 and 8.5).
11 Peatland areas expansion, shrinkage, and C accumulation and decomposition are ~~modeled~~ modelled. In the 21st century,
12 northern peatlands are projected to be a C source of 1.2-13.3 Pg C under all climate scenarios except for RCP 2.6 of bcc-
13 csm1-1 (a sink of 0.8 Pg C). During 2100-2300, northern peatlands under all scenarios are a C source under IPSL-CM5A-LR
14 scenarios, being larger sources than bcc-csm1-1 scenarios (5.9-118.3 vs. 0.7-87.6 Pg C). ~~The peatland being C sources are~~
15 ~~due to C sources are attributed to:~~ 1) peatland water table depth (WTD) becomes deeper and permafrost thaw increases
16 decomposition rate; 2) net primary production (NPP) does not increase much as climate warms because peat drying
17 suppresses net N mineralization, and 3) as WTD deepens, peatlands switches from moss-herbaceous dominated to moss-
18 woody dominated, while woody plants require more N for productivity. Under IPSL-CM5A-LR scenarios, northern
19 peatlands remain as a C sink until pan-Arctic annual temperature reaches -2.6 - -2.89°C, while this threshold is -2.09 - -
20 2.35°C under bcc-csm1-1 scenarios. This study predicts ~~an earlier an~~ -northern peatland sink to source shift in around 2050,
21 earlier than previous estimates ~~of after 2100 in the literature~~ and emphasizes the vulnerability of northern peatlands to
22 climate change.

23 1 Introduction

24 Peatlands are an ecosystem type that characteristically has more than 30cm peat thickness comprised of more than
25 30% organic materials within the peat layer (Finlayson and Milton, 2018). The formation of this thick organic soil layer
26 requires wet and low oxygen conditions that prevent dead plant litter from being fully decomposed (Finlayson and Milton,
27 2018). Around 85% of global peatlands C storage is in northern high latitude regions (415±150 Pg C) (Nichols and Peteet,
28 2019; Turunen et al., 2002) where low temperature and relatively high precipitation create favorable conditions for peat
29 accumulation (Xu et al., 2018; Hugelius et al., 2020).

30 Peatlands are vulnerable to disturbances induced by climate warming (Loisel et al., 2021), especially when the
31 warming in the Arctic region ~~is more severe than in other regions~~ ~~is almost three times as much as the global average~~ (Allen
32 ~~et al., 2018, GISTEMP-Team., 2021~~). First, warming influences northern terrestrial ecosystem vegetation productivity by
33 increasing spring photosynthesis, ~~triggering spring onset earlier and delaying autumn green-down and prolongs growing~~
34 ~~season~~ (Piao et al., 2008; Helbig et al., 2017, Richardson et al., 2018). Second, warming could induce drier Arctic conditions
35 ~~with 21% of lake count and 2% of lake area decrease found from the during 1960s to present~~ (Finger Higgins et al., 2019),
36 and peatlands water table drawdown ~~would~~ result in net increase of greenhouse gas emissions ~~of 0.86 Gt CO₂-eq .yr⁻¹ by~~
37 ~~2100~~ (Huang et al., 2021). Third, decomposition rate increases under higher temperature and previous studies found positive
38 linear correlations between warming and net C loss rate ~~of 31.3 gC.m⁻².year⁻¹.°C⁻¹~~ (Hanson et al., 2020). Fourth, permafrost
39 thaw under warming conditions will expose previously-frozen C for ~~dissolving and~~ decomposition (Gandois et al., 2019). To
40 date, multiple ~~modelling~~ studies have explored northern peatland responses to future climate changes (Loisel et al., 2021;
41 Qiu et al., 2020; Chaudhary et al., 2020; Müller and Joos, 2021). However, the projection of northern peatland C sink
42 capacity during the 21st century is highly diverse including sink-to-source switch (Chaudhary et al., 2017; Müller and Joos,
43 2021), higher sink capacity under mild climate changes (Qiu et al., 2020), and the reduced C sink capacity (Chaudhary et al.,
44 2020).

45 Given the uncertainties of northern peatlands response to future climate changes, ~~modeling~~ ~~modelling~~ peatland C
46 dynamics ~~considering including~~ peatland extent changes could improve the accuracy of future projection. In this study, a
47 process-based model, the Peatland Terrestrial Ecosystem Model (PTEM 2.2), is used to address this issue. PTEM 2.0 has been
48 modified in terms of plant functional type (PFT), peat accumulation and decomposition, fen-bog transition and soil thermal
49 module to better represent peatland ecosystem processes (Zhao et al., 2022b). The revised PTEM 2.0 is able to capture peat
50 core age-depth profile at site level (Zhao et al., 2022b) and has been further modified and applied to simulate Holocene
51 (PTEM 2.1, 15ka BP - 1990) pan-Arctic peatland accumulation and expansion at 0.5° resolution (Zhao et al., 2022a). The
52 estimated pan-Arctic peatland C stock is 396-421 Pg C and Holocene average C accumulation rate (CAR) is 22.9 g C.m⁻².yr⁻¹
53 (Zhao et al., 2022a). The values and spatial pattern of soil C stock are in a close agreement with Qiu et al. (2019), Hugelius
54 et al. (2020), Spahni et al. (2013) and Hugelius et al. (2013), and the values and temporal pattern of CAR are consistent with
55 Loisel et al. (2014), Chaudhary et al. (2020) and Nichols and Peteet (2019). In this study, the results of the Holocene
56 simulation are used as the initial condition for the future simulation.

57 The methods used in Holocene simulation can not be applied directly to future simulation due to two issues. First,
58 previous studies on future peatland C dynamics are mostly based on fixed peatland extent (Loisel et al., 2021; ~~Qiu et al.,~~
59 ~~2020; Chaudhary et al., 2020; Müller and Joos, 2021~~), ~~but future. However, the future~~ peatland extent is likely to vary
60 under climate change. To address this issue, we enhance PTEM 2.2 to simulate wetland dynamic extent during 1990-2300 at
61 sub-grid cell scales. Notably, although the spatially explicit peat expansion process was considered in the Holocene
62 simulation, the sub-grid cell expansion trend was simply derived from the fitted curve of existing pan-Arctic peat basal dates
63 (Zhao et al., 2022a). It is problematic to apply this fitted trend to future simulation since severe climate changes may

Formatted: Superscript

Formatted: Superscript

Formatted: Superscript

Formatted: Superscript

Formatted: Superscript

64 interrupt the Holocene peat expansion pattern. Therefore, a different approach of estimating peatland extent needs to be
65 developed for future simulation.

66 Second, in PTEM 2.2, peatland water table depth (WTD) and nutrient availability is influenced by run-on, which is
67 the water input from ground water or adjacent water bodies into the peatlands. Previous PTEM 2.1 assumes run-on is a
68 function of peat thickness, and the theoretically maximum run-on ~~when corresponding with 0cm peat thickness is set to 0~~
69 ~~cm~~. Under relatively stable climate conditions during the Holocene after peat initiation, the theoretically maximum run-on is
70 assumed to be a constant (i.e., parameter) and thereby run-on solely depends on peat thickness (Zhao et al., 2022a).
71 However, when climate becomes wetter or drier in the future, the theoretically maximum run-on could vary significantly and
72 the original PTEM 2.1 assumption becomes problematic. Therefore, it is necessary to revise the hydrology module of PTEM
73 2.2 such that run-on could respond to climate change.

74 To address these two issues, a TOPMODEL approach is used (Lu and Zhuang (2012)). The TOPMODEL approach
75 downscales coarse grid cell WTD into finer resolutions given the sub-grid-cell topographic wetness index (TWI) and decay
76 parameter (f) (Beven and Kirkby, 1979). Previous studies have combined TEM, TOPMODEL and variable infiltration
77 capacity (VIC) model to estimate Alaska Yukon river basin methane emissions using 1km resolution WTD interpolated from
78 30km resolution (e.g., Lu and Zhuang (2012)). By applying TOPMODEL, we are able to estimate the dynamics of a) sub-
79 grid-cell WTD; b) the spatially explicit wetland fraction defined by annual WTD threshold (25cm, Fan et al. (2013)); c) sub
80 grid-cell peat accumulation and decomposition given interpolated WTD; and d) the spatially explicit peatland fraction
81 defined by peat thickness threshold (30cm, Finlayson and Milton (2018)). Furthermore, soil moisture can be estimated from
82 WTD, with which we can estimate run-on from the difference between interpolated WTD and simulated WTD without run-
83 on.

84 With peatland dynamics being simulated both horizontally (i.e., peatlands expansion and shrink) and vertically (i.e.,
85 peat accumulation and decomposition), this study aims to answer the following questions: a) how will the C sink of pan-
86 Arctic peatlands change during 1990-2300? b) What are the major drivers for these changes? c) How does the pan-Arctic
87 peatlands C sink respond to unit temperature and precipitation increase? and d) What is the threshold temperature and
88 precipitation for pan-Arctic peatland C sink and source shift?

89 2 Methods

90 In this study, two CMIP5 climate model products (IPSL-CM5A-LR and bcc-csm1-1) are selected as climate inputs,
91 with three warming scenarios considered (RCP 2.6, RCP 4.5 and RCP 8.5). The simulation is divided into two parts: 1)
92 simulating grid cell average WTD with PTEM 2.2 and interpolating grid cell WTD into sub-grid cell scale with the
93 TOPMODEL approach; and 2) simulating sub-grid cell scale peat accumulation and decomposition in current and potential
94 peatland regions (Figure 1). Although this study aims at the peatland C expansion, shrinkage, accumulation and

95 [decompositiondynamics](#) after 1990, the simulations start in 1940. The simulation during 1940-1990 works as spin up process
96 and is also used for calibration against historical data.

97 2.1 Selection of climate input data

98 In the previous PTEM 2.0 site-level simulation, among many CMIP5 data products, IPSL-CM5A-LR product was
99 selected as climate input because it provides long temporal coverage (1850-2300) for RCP 2.6, RCP 4.5 and RCP 8.5
100 scenarios (Zhao et al., 2022b). In addition, it shows a good agreement with [Climatic Research Unit \(CRU\)](#)CRU temperature
101 in Eurasia and low biases in historical temperature and precipitation in North America (Miao et al., 2014; Sheffield et al.,
102 2013). However, IPSL-CM5A-LR product also shows more extreme warming than the other CMIP5 products, especially
103 under RCP 8.5 (Palmer et al., 2018). To address the uncertainty caused by climate inputs, another CMIP5 product, bcc-
104 csm1-1, covering 1850-2300, three RCP scenarios, projecting milder future climate warming, is selected. [The comparison of](#)
105 [two forcing datasets is provided in SI Table1](#). In order to run PTEM 2.2, temperature, precipitation, cloudiness and vapor
106 pressure are required. Neither of IPSL-CM5A-LR and bcc-csm1-1 model provides vapor pressure data, which are thus
107 calculated with temperature and relative humidity (Zhao et al., 2022b). Both climate products are bias-corrected to [Climatic](#)
108 [Research Unit](#)CRU data (v4.03, Harris et al. (2014)) during 1940-1990 as described in Zhao et al. (2022b). The bias
109 correction makes sure that the difference in future simulations under two climate inputs are mostly introduced by the
110 different level of post-1990 warming, rather than the difference in their historical records before 1990.

111 **Table 1.** List of abbreviations

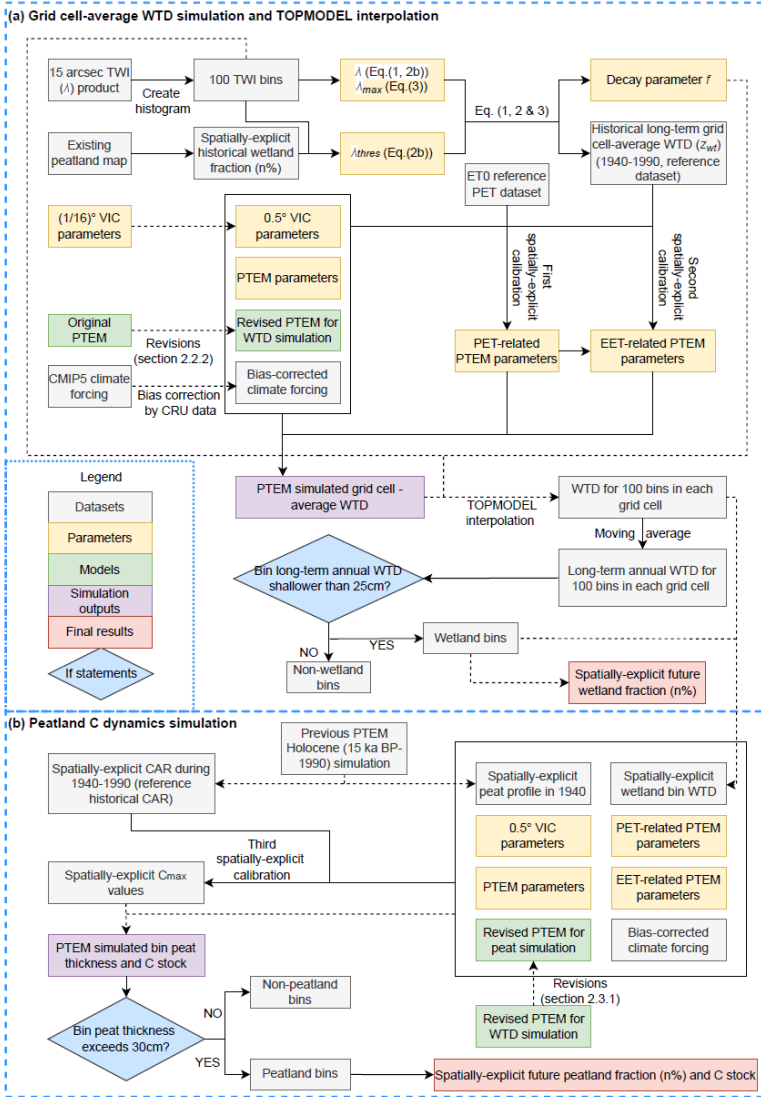
<u>Abbreviation</u>	<u>Full name</u>
PTEM	Peatland terrestrial ecosystem model
CMIP5	Coupled Model Intercomparison Project Phase 5
RCP	Representative Concentration Pathway
WTD	Water table depth
CAR	C accumulation rate
VIC	Variable Infiltration Capacity model
TWI	Topographic wetness index
PFT	Plant functional type
EET	Evapotranspiration
PET	Potential evapotranspiration
PEST	Model-Independent Parameter Estimation and Uncertainty Analysis
NPP	Net primary productivity

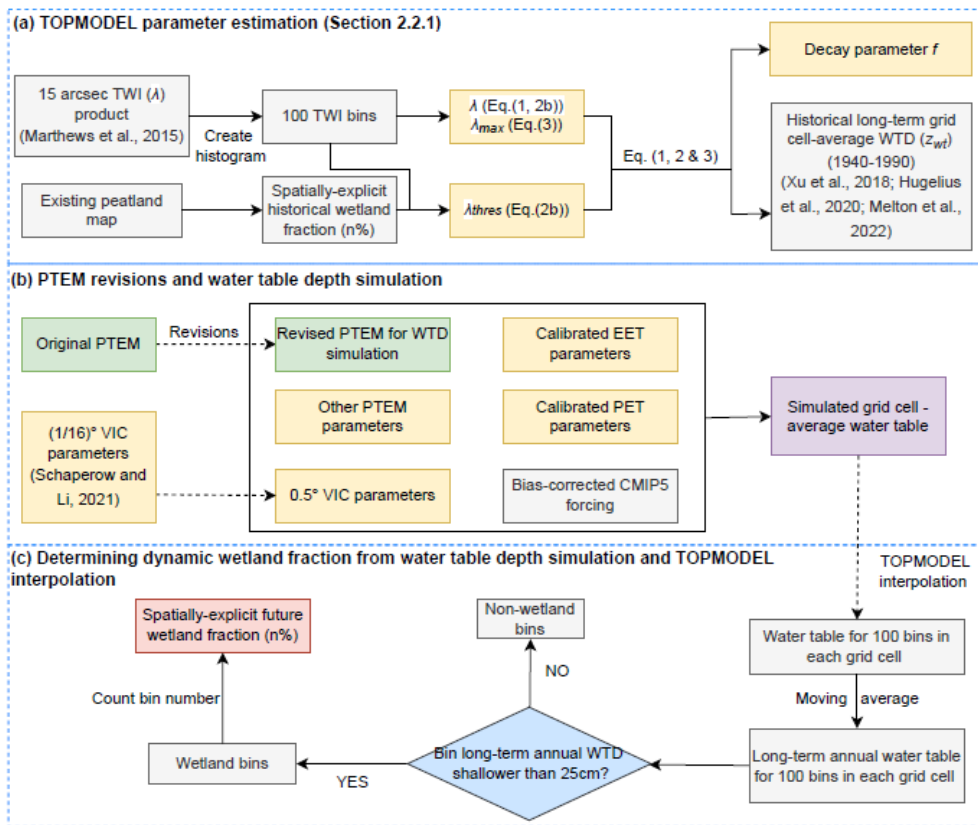
Formatted: Font: 10 pt

Formatted Table

Formatted Table

112





114

115 Figure 1. Flow chart of Method Section 2.2 and 2.3.

116

117 **2.2 Future grid cell average WTD simulation**

118 **2.2.1 TOPMODEL parameter estimation**

119 In this study, the peatland condition in 1940 derived from previous Holocene simulation is used as the initial
 120 condition for future peatland simulations (1940-2300) (Zhao et al., 2022a). In order to be consistent with the Holocene
 121 simulation, before running future WTD simulation, it is necessary to make sure that interpolating the PTEM-simulated recent
 122 WTD by TOPMODEL could derive the wetland extent as shown in the end of the Holocene simulation. In particular,
 123 ‘recent’ in this study refers to 1940-1990, and wetlands are defined as the region with long-term annual WTD shallower than

124 25cm (Fan et al., 2013). To satisfy this requirement, the TOPMODEL parameters need to be estimated before WTD
 125 simulation (Figure 1(a)). TOPMODEL describes sub-grid cell WTD variation with topography. The topography effects on
 126 the local WTD are estimated with topographic wetness index (TWI) values, the larger TWI values indicate the shallower
 127 WTD and higher flooding probability (Stocker et al., 2014). In order to estimate sub-grid cell wetland and peatland
 128 conditions at 1% accuracy, each $0.5^\circ \times 0.5^\circ$ grid cell is divided into 100 bins by the TWI histogram (Figure 1 (a), SI Figure1).
 129 With global terrestrial TWI values available at 15 arcsec resolution (Marthews et al., 2015), each bin is composed of 36 TWI
 130 values where water bodies have null values (SI Figure1). For bin i within a given grid cell:

$$131 \quad z_{wti} = z_{wt} - \frac{1}{f} \times (k_i - \lambda) \quad (1)$$

132 Where z_{wti} is the WTD of bin i , k_i is the average TWI of bin i , λ is the grid cell average TWI, z_{wt} is the grid cell
 133 average WTD and f is the decay parameter. In Eq. (1), the parameters need to be estimated are z_{wt} and f . In particular, the
 134 z_{wt} here refers to the 50-year average WTD during 1940-1990. z_{wt} and f values are calculated as:

$$135 \quad \begin{cases} f = 2.6 & (2a) \\ z_{wt-thres} = z_{wt} + \frac{1}{f}(\lambda_{thres} - \lambda) & (2b) \end{cases}$$

136
 137 Where f value is from Kleinen et al. (2020). $z_{wt-thres}$ is the threshold WTD of wetlands (i.e., -0.25m) and λ_{thres} is
 138 the TWI value corresponding to $z_{wt-thres}$. For a given grid cell where wetland abundance is $n\%$ (n is an integer), λ_{thres} is
 139 the TWI value of the n -th largest TWI values among 100 bins. The spatially explicit wetland fraction ($n\%$) during 1940-1990
 140 is consistent with the wetland fraction in 1990 in the Holocene simulation, which is the average value of three peatland maps
 141 covering the pan-Arctic region (Xu et al., 2018; Hugelius et al., 2020; Melton et al., 2022). The shallowest WTD in each grid
 142 cell is:

$$143 \quad z_{wt-max} = z_{wt} + \frac{1}{f}(\lambda_{max} - \lambda) \quad (3)$$

144 Where λ_{max} is the maximum TWI value in 100 bins. If z_{wt-max} is greater than zero (i.e., above surface), z_{wt-max}
 145 is assumed to be -0.01m, and z_{wt} and f values are calculated by Eq. (2b) and Eq. (3). Otherwise, z_{wt} and f values are
 146 calculated by Eq. (2a) and Eq. (2b).

147 2.2.2 PTEM revisions

148 The PTEM 2.1 used in pan-Arctic Holocene simulations is able to estimate the wetland WTD in a given grid cell,
 149 while not the grid-cell average WTD composed of both wetland and non-wetland land covers (Zhao et al., 2022a). In order
 150 to simulate the grid-cell average WTD, PTEM 2.1 is revised by applying some of the algorithms from VIC model (Figure
 151 1(b)). VIC model was developed by Liang et al. (1994) and has been updated to version 5 (VIC-5, Hamman et al. (2018)).
 152 Compared with the hydrology module of PTEM 2.1, VIC has the same soil vertical structure of three layers. The major
 153 hydrological processes including canopy interception of precipitation, infiltration, gravity-driven vertical flow,
 154 evapotranspiration, upper soil layer evaporation, effect of frozen-thaw on soil moisture are considered in both models (Liang
 155 et al., 1994; Zhuang et al., 2002). With similar structure, processes and variables, it is possible to apply some of VIC

156 algorithms to PTEM 2.1. In particular, the algorithms of surface runoff, vertical flow from upper to lower layers, the
 157 computation of base flow and the estimation of WTD from given soil moisture are added to PTEM 2.1. The computation of
 158 surface runoff in VIC is based on the Xinanjiang model that assumes runoff is the amount of precipitation that falls on the
 159 saturated fraction of a grid cell (Zhao et al., 1980). The relationship between soil water storage and saturated fraction is
 160 given by:

$$161 \quad i = i_m [1 - (1 - A)^{1/B}] \quad (4)$$

162 Where A is the fraction of the grid cell that the infiltration capacity (i.e., the possible maximum depth of water
 163 stored in soil column given area fraction) is less than i , i_m is the maximum infiltration capacity within the given grid cell,
 164 and B is a shape parameter (Wood et al., 1992). The calculation of the uppermost layer runoff given precipitation and the
 165 initial soil moisture is well documented in Wood et al. (1992) (Eq. (1-3)) and Liang et al. (1994) (Eq. (13), Eq. (17-18)). In
 166 addition, gravity-driven water flow from upper to lower layers is given by Liang et al. (1994) (Eq. (18-20)) based on upper
 167 layer soil moisture, residual moisture content, pore size distribution index and the hydraulic conductivity estimated from
 168 Brooks (1965). Following VIC, PTEM 2.2 also assumes base flow only happens in the bottom soil layer. The computation of
 169 base flow in VIC is derived from the model in Franchini and Pacciani (1991) and the equations are listed in Liang et al.
 170 (1994) (Eq. (21)). Computing WTD given soil moisture was first used in VIC 4.1.2 (Bohn et al., 2013). Edited from VIC-5,
 171 the WTD-soil moisture relationship in PTEM 2.2 is given by:

$$172 \quad W_{tot} = W_{avg} \times (SM_{max} - SM_{res}) + SM_{res} \quad (5)$$

173 Where W_{tot} is the total soil moisture of three layers (mm), W_{avg} is the average relative soil moisture, SM_{max} is the
 174 maximum soil moisture (mm) and SM_{res} is the residual soil moisture (mm). With SM_{max} and SM_{res} being spatially explicit
 175 parameters, W_{avg} is:

$$176 \quad W_{avg} = (D_{tot} - z_{wt} - \frac{b}{b-1} \times bubble \times (1 - (\frac{z_{wt} + bubble}{bubble})^{\frac{b-1}{b}})) / D_{tot} \quad (6)$$

177 Where D_{tot} is the total depth of soil layer (cm), z_{wt} is given WTD (cm below surface), $bubble$ is the bubbling
 178 pressure (cm), b is the parameter:

$$179 \quad b = 0.5 \times (expt - 3) \quad (7)$$

180 Where $expt$ is the exponent parameter from Brooks-Corey relationship, and is always greater than 3 (Rawls et al.,
 181 1992). In PTEM 2.2, the spatially explicit relationship between WTD and total soil moisture is given by Eq. (5-7) at 5cm
 182 WTD interval. During simulation, PTEM 2.2 calculates the total soil moisture and finds the corresponding WTD. In case of
 183 soil moisture does not correspond with any 5-cm interval WTD, PTEM 2.2 will find the closest upper and lower soil
 184 moisture values in the soil moisture-WTD profile and interpolate from the upper and lower WTD values.

185 In site-level and Holocene simulations, there are three PFTs in PTEM 2.0 and 2.1: moss, herbaceous plant and
 186 shrub (Zhao et al., 2022b). However, trees are also an important PFT in northern peatlands (Hanson et al., 2020). Therefore,
 187 in both grid-cell average WTD and sub-grid cell peatland simulations, it is necessary to include trees as a PFT. In particular,
 188 the vegetation C and N pool in PTEM 2.2 are now divided into four sub-pools: moss, herbaceous plant, shrub and tree. The

189 dominance of these four PFTs are determined by WTD and their maximum possible productivity. The litter fall from four
 190 PFTs becomes the input of soil C and N, and the decomposition ability of litter is influenced by the fraction of litter origin
 191 from each PFT. The calculations of C and N cycles of trees are the same as the other three PFTs, although controlled by
 192 different PFT-specific parameters. The detailed description and equations are documented in Zhao et al. (2022b).

193 The calculation of evapotranspiration (EET) of vascular plants in PTEM 2.2 is derived from Food and Agriculture
 194 Organization (FAO)FAO algorithm for calculating crop EET (Allen et al., 1998):

$$195 \ EET = PET \times k_c \times foliage + E_{soil} \times (1 - foliage) \quad (8)$$

196 Where PET is the potential evapotranspiration given by Penman-Monteith model in PTEM 2.2, k_c is a coefficient,
 197 E_{soil} is the evaporation from the top soil layerbare land and $foliage$ is a PTEM 2.2 variable describing the relative
 198 abundance of leaf biomass (0-1). $E_{soil} \times (1 - foliage)$ is used to represent the evapotranspiration from the top
 199 hydrology layer, which is assumed to be a moss layer in PTEM. Although the Food and Agriculture OrganizationFAO
 200 algorithm is widely applied in estimating crop EET, it is also proved applicable to shrubland, grassland and forest (Liu et al.,
 201 2017). In PTEM 2.2, k_c is calculated as:

$$202 \ k_c = \sum_{i=1}^3 k_{c-pft} \times w_{pft} \quad (9)$$

203 Where three vascular PFTs are considered influential to EET (i.e., herbaceous plant, shrub and tree), k_{c-pft} is the
 204 spatially explicit coefficient for given PFT, and w_{pft} is the weight of given PFT estimated from its dominance:

$$205 \ w_{pft} = \frac{VEGC_{pft}}{\sum_{i=1}^3 VEGC_{pft}} \quad (10)$$

206 Where $VEGC_{pft}$ is the vegetation C of given PFT, and only three vascular PFTs are used for weight calculation. In
 207 WTD simulation, we assume no run-on from adjacent grid cells, thereby the grid cell water balance is:

$$208 \ \Delta SM = P - R_{off} - B - EET \quad (11)$$

209 Where ΔSM is the change of soil moisture, P is precipitation, R_{off} is surface run-off and B is the bottom layer base
 210 flow.

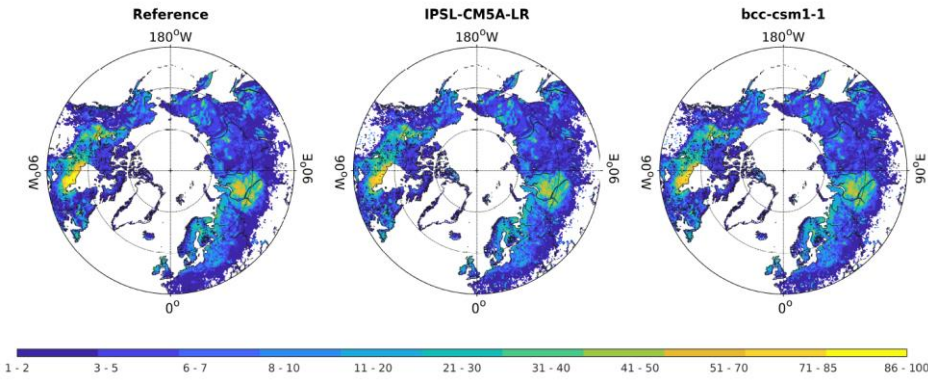
211 2.2.3 Grid cell average WTD simulation and post-processing

212 Adding VIC algorithms to PTEM 2.2 requires VIC parameters at 0.5° resolution. These parameters include variable
 213 infiltration curve parameter (binfilt), maximum velocity of base flow (Dsmax), fraction of Dsmax where non-linear base
 214 flow begins (Ds), fraction of maximum soil moisture where non-linear base flow occurs (Ws), exponent used in base flow
 215 curve (c), expt in Eq. (7), saturated hydrologic conductivity (Ksat), depth of three soil layers (depth), bubbling pressure of
 216 soil layers (bubble), bulk density of soil layers (bulk_density) and soil particle density (soil_density). These parameter values
 217 are available globally at (1/16)° resolution (Schaperow and Li, 2021) and are aggregated into 0.5° resolution in this study. To
 218 run PTEM 2.2, in addition to the climate inputs, the historical (1940-1990) CO₂ concentration (ppm) is derived from TraCE
 219 21ka dataset (He, 2011). The CO₂ concentration for three RCP scenarios (1991-2300) is provided by Meinshausen et al.
 220 (2011). Spatially explicit soil texture (FAOa6/UNESCOnesso, 1974) and elevation (Zhuang et al., 2002) were also required
 221 (Figure 1(b)).

222 Before conducting WTD simulation, spatially explicit calibration for annual PET and k_{c-pft} are conducted.
223 Spatially explicit calibration for annual PET is conducted because the original PTEM 2.1 parameters estimate unreasonably
224 large PET. Therefore, the global aridity index and potential evapo-transpiration (ET0) database v3 (Zomer and Trabucco,
225 2022) is selected as a reference. The dataset is selected because its annual PET is the long-term value of 1970-2000, which
226 can be the approximate reference to the PET during 1940-1990 in this study. In addition, the reference dataset is also based
227 on Penman-Monteith model but with more detailed estimation on the parameters than PTEM (Zomer and Trabucco, 2022).
228 The 30 arcsec resolution reference PET is aggregated into 0.5° resolution for calibration. The spatially explicit Penman-
229 Monteith parameters in PTEM 2.2 are calibrated with PEST (v17.2 for Linux). Since both reference dataset and PTEM 2.2
230 estimate PET with the same model, the calibration result is close to the reference for both IPSL-CM5A-LR and bcc-csm1-1
231 climate inputs (SI Figure 24).

232 After PET calibration, the spatially explicit calibration for k_{c-pft} is conducted such that the 50-year WTD is
233 consistent with the z_{wt} calculated by Eq. (2-3). Same as PET calibration, spatially explicit k_{c-pft} values are also calibrated
234 by PEST (v17.2 for Linux). The wetland abundance in the end of the Holocene simulation (i.e., reference dataset) (Xu et al.,
235 2018; Hugelius et al., 2020; Melton et al., 2022) and the wetland abundance interpolated by TOPMODEL from calibrated
236 WTD (average of 1940-1990) is shown in SI-Figure 2. Notably, the extent of pan-Arctic peatlands is used as an
237 approximation of pan-Arctic wetlands because the northern peatland extent is estimated to be 2.9-3.3 Mkm², with an average
238 of 3.05 Mkm² (Xu et al., 2018; Hugelius et al., 2020; Melton et al., 2022); while the northern wetland extent is estimated to
239 be 3.2 Mkm² (Olefeldt et al. 2021), indicating northern wetlands are dominated by northern peatlands. In addition, the
240 peatland coverage from Xu et al. (2018) and Hugelius et al.(2020) both include the shallow peats (<30cm), which is
241 classified as wetlands rather than peatlands in this study. Since each grid cell is divided into 100 bins by TWI values, the
242 minimum wetland abundance is 1%. In this study, the grid cells with less than 1% wetland are not used for peat simulation.
243 Leaving out the grid cells with less than 1% wetlands, the pan-Arctic wetlands area for the reference dataset is 2.93 Mkm²,
244 the calibrated wetlands area with IPSL-CM5A-LR forcing input is 2.81 million km², and with bcc-csm1-1 forcing input is
245 2.86 million km² (Figure 2).

246 After calibration, the WTD simulation is conducted for 1940-2300 at 0.5° resolution (Figure 1 (ba)). Notably, WTD
247 simulation only aims at estimating grid cell average WTD and the peat accumulation and decomposition processes are not
248 simulated. The grid cell average WTD during 1940-2300 is interpolated by TOPMODEL using the parameters calculated in
249 Section 2.2.1 (Figure 1(c)). The changes of wetlands extent during 1990-2300 under IPSL-CM5A-LR and bcc-csm1-1
250 forcing inputs are presented in SI Figure 3 and 4.



251 **Figure 2.** Comparison between the reference and calibrated wetland abundance (%) during 1940-1990 interpolated with
 252 TOPMODEL approach. The reference dataset is the average peatland abundance of three peatland maps (Xu et al., 2018;
 253 Hugelius et al., 2020; Melton et al., 2022), and calibration is conducted for IPSL-CM5A-LR and bcc-csm1-1 climate inputs,
 254 respectively. The grid cells with less than 1% wetlands are left blank. This is the initial wetland extent for future peatland
 255 simulation.

257 2.3 Peatland simulation

258 2.3.1 PTEM revision

259 The TOPMODEL-interpolated bin WTD is used as an input in peatland simulation (Figure 1 (b)). In contrast to the
 260 WTD simulation where the grid cell run-on is assumed to be zero (Eq. (11)), the run-on in peatland simulation is calculated
 261 with a water balance equation:

$$262 \Delta SM = P + R_{on} - R_{off} - B - EET \quad (12)$$

263 Where ΔSM is the difference between soil moisture at two adjacent time steps (i.e., months), and the soil moisture
 264 in each month is estimated from the input WTD and the WTD-soil moisture relationship given by Eq. (5-7). The run-off
 265 (R_{off}), base flow (B) and evapotranspiration (EET) are calculated in the same way as in WTD simulation. pH values are
 266 influential to CH_4 production process and is simulated in both Holocene simulation and the future simulations. In the
 267 Holocene simulation, soil pH value is calculated as a function of run-on which is solely controlled by peat thickness. In the
 268 revision, soil pH is calculated as:

$$269 pH = -\log_{10}(n^{H^+}/SM) \quad (13)$$

270 Where pH is the soil pH value, n^{H^+} is the number of H^+ particles, and SM is the soil moisture (mm). Notably, on
 271 unit area (i.e., $1m^2$), 1mm soil moisture is equal to 1L soil water. Therefore, n^{H^+}/SM calculates the concentration of H^+
 272 particles per liter. And the number of H^+ particles is calculated as:

Formatted: Indent: First line: 0"

Formatted: Font: (Default) Times New Roman, (Asian) SimSun, Kern at 16 pt

273
$$\Delta H^+ = 10^{-pH_p} \times P + 10^{-pH_{ron}} \times R_{on} - 10^{-pH_w} \times EET - 10^{-pH_0} \times (R_{off} + B) \quad (14)$$

274 Where pH_p is the pH value of precipitation (assumed 5.0), pH_{ron} is the pH value of run-on water (assumed 7.0),
275 pH_w is the pH value of EET water (assumed 7.0), and pH_0 is the pH value of soil water at previous month. The spatially
276 explicit initial pH values are from (Carter and Scholes, 2000).

277 In Holocene simulations, CH₄ production is simulated, but since oxidation process is not considered, CH₄ emission
278 is not calculated. In this revision, CH₄ oxidation is enabled and thereby it is possible to estimate net CH₄ emission. The
279 algorithms are documented in Zhuang et al. (2004).

280 2.3.2 PTEM simulation

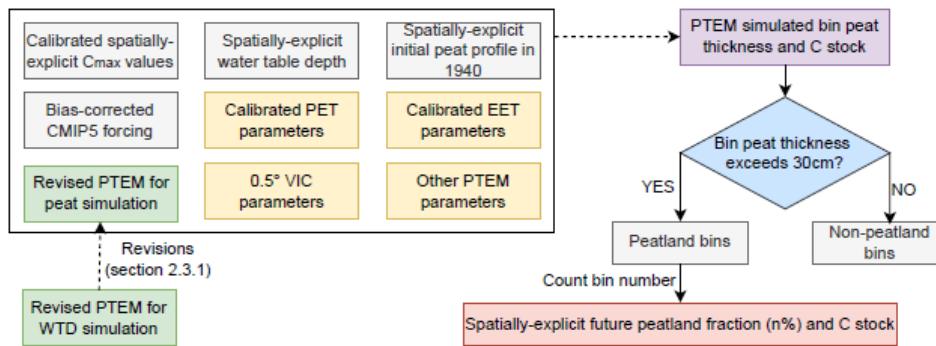
281 In each grid cell, among the 100 bins classified by TWI, the bins that the long-term WTD has ever been shallower
282 than 25cm are classified as 'potential peatlands', which are used for peatland simulation ~~(Figure 1 (b))~~. To be consistent with
283 the WTD simulation, long-term WTD refers to the 50-year moving average of annual WTD. In this study, we assume within
284 each grid cell, the climate conditions are similar and the key control of whether peat exists at sub-grid cell scale is the local
285 WTD influenced by sub-grid topography. Therefore, for all the bins in the same 0.5°×0.5° grid cell, the forcing data, soil
286 texture, elevation and parameters are the same except for the input WTD.

287 In Holocene simulations, the maximum C assimilated by ecosystem parameter (c_{max}) is calibrated for over 2000
288 peat cores and interpolated into the pan-Arctic region (Zhao et al., 2022a). The calibration process reduces the uncertainty
289 from forcing data, other parameters and model structure, and the simulated spatial and temporal pattern of pan-Arctic
290 peatland C stock is consistent with multiple datasets (Zhao et al., 2022a). However, since the hydrology module of PTEM
291 2.2 is revised and peat accumulation and decomposition is sensitive to hydrological processes, using the original parameters
292 could result in considerable bias. In order to make sure the revised PTEM 2.2 simulates consistent C accumulation rate
293 (CAR) with the previous study, a spatially explicit calibration on maximum C assimilated by ecosystem (c_{max}) parameter is
294 conducted.

295 Before calibrating CAR, it is necessary to initialize PTEM 2.2 with reasonable peat conditions. To initialize the
296 simulation, the peat profile in 1940 derived from the Holocene simulation (Zhao et al., 2022a) is used ~~(Figure 3-1 (b))~~. In
297 particular, the peat profile records the physical property of vertical peat layers including bulk density, organic C density,
298 layer thickness (1cm except for the top layer), fraction of remaining undecomposed organic matter and decomposition rate of
299 undecomposed organic matter at 0°C. This information can be used to estimate the decomposition rate of existing peat given
300 WTD, soil pH and soil temperature (Zhao et al., 2022b).

301 With initial peat profile as an input, c_{max} values are calibrated with PEST (v17.2 for Linux) ~~(Figure 1 (b))~~. In
302 particular, within each grid cell, the 50-year average CAR of historical wetland bins (i.e., the bins that are classified as
303 wetlands during 1940-1990) are simulated and averaged to get the grid cell average 50-year peatland CAR. This grid cell
304 average peatland CAR is calibrated against the CAR derived from the Holocene simulation during the same period (SI
305 Figure 5).

306 After calibration, the peat simulation is conducted for all pan-Arctic potential peatland bins during 1940-2300
 307 (Figure 21-(b)). For the Greenland grid cells not included in the Holocene simulation and thereby have no calibrated c_{max}
 308 values, the c_{max} values are interpolated from adjacent grid cells. For the bins not included in the Holocene simulation or not
 309 being peatlands before 1990, the peat profile is initialized as 3cm fully decomposed peat. Notably, under different forcing
 310 data and warming scenarios, the number and distribution of potential peatland bins are slightly different, which makes the
 311 initial pan-Arctic peatland C storage in 1940 slightly different (SI Table 24). When running peat simulation, the forcing input
 312 (temperature, precipitation, cloudiness and vapor pressure), soil texture, elevation and parameters are the same as the ones
 313 used in the WTD simulation, except for the spatial-explicit c_{max} values.



314
 315 **Figure 3. Flow chart of Method Section 2.3.2.**

316 **2.3.3. Peat simulation post-processing**

317 After simulation, the simulated results are analyzed in terms of 1) the temporal pattern of pan-Arctic climate
 318 dynamics; 2) the temporal pattern of pan-Arctic peatland C stocks and C fluxes; 3) the main drivers of pan-Arctic peatland C
 319 dynamics; and 4) the threshold temperature and precipitation needed to transition the peatland from a C sink to a C source
 320 pan-Arctic C sink/source shift.

321 Threshold temperature is calculated with logistic regression:

$$322 f(temp) = \begin{cases} 0 & \text{Net ecosystem productivity } NEP \leq 0 \\ 1 & \text{Net ecosystem productivity } NEP > 0 \end{cases}$$

323 (15)

324 Where NEP is net ecosystem productivity. A fitting curve of $f(temp)$ is derived for the pan-Arctic region and for
 325 each grid cell. Under sink-source shift, the fitting curve rises from 0 to 1, and the threshold temperature of sink-source shift
 326 is determined when $f(temp)$ is 0.5. The threshold precipitation and threshold number of annual unfrozen days is calculated

Formatted: Indent: First line: 0"

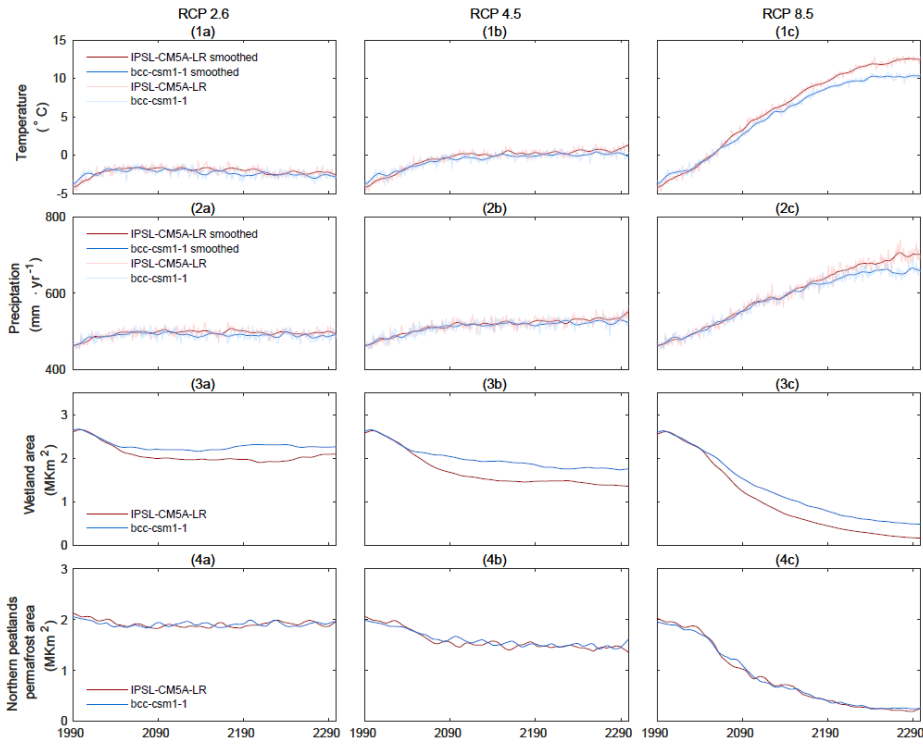
Formatted: Font: (Default) Times New Roman, 9 pt, Bold
 Font color: Gray-85%

327 in the same way. In particular, to estimate the number of unfrozen days, the daily temperature is reconstructed from monthly
328 temperature by the algorithms used in Zhao et al. (2022a).

329 3. Results

330 3.1 Warmer and drier pan-Arctic peatlands during 1990-2300

331



332

333 Figure 42. Time series of pan-Arctic annual air temperature ($^{\circ}\text{C}$), annual precipitation ($\text{mm}\cdot\text{yr}^{-1}$), wetland area (Mkm^2) and
334 permafrost area in peatland regions (Mkm^2) during 1990-2300.

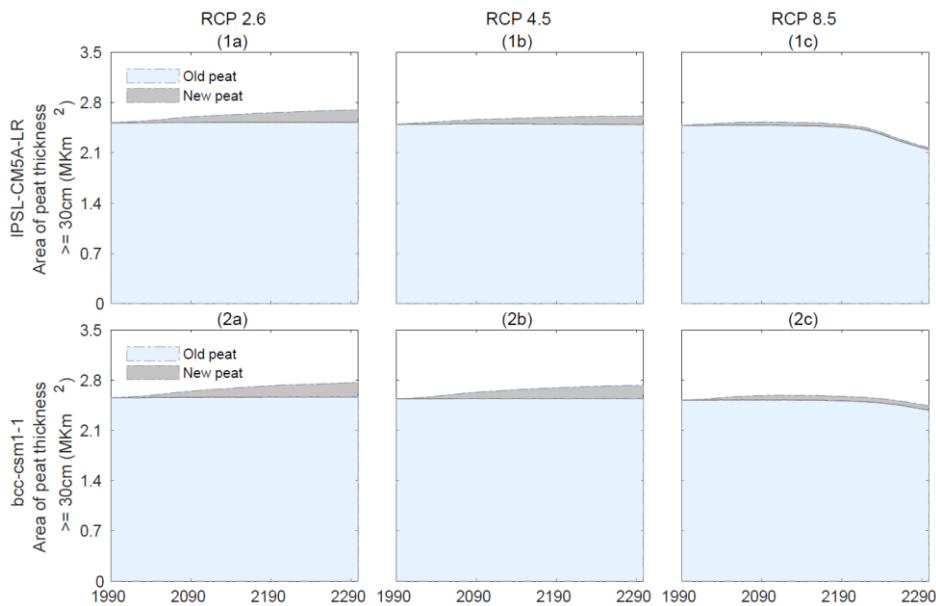
335 Both IPSL-CM5A-LR and bcc-csm1-1 climates show **increasinghigher** temperature and precipitation during 1990-
336 2300. In particular, under RCP 2.6 and RCP 4.5, temperature increases mostly before 2100 by 2.3-4.1 $^{\circ}\text{C}$ and 2.0-3.2 $^{\circ}\text{C}$ under
337 IPSL-CM5A-LR and bcc-csm1-1, respectively (Figure 42 1(a-b), SI Table 32). Meanwhile, precipitation increases by 40.7-
338 59.7 $\text{mm}\cdot\text{yr}^{-1}$ and 38.1-53.9 $\text{mm}\cdot\text{yr}^{-1}$ for under IPSL-CM5A-LR and bcc-csm1-1 (Figure 2-4 2(a-b), SI Table 23). During
339 2100-2300, under RCP 2.6, the temperature decreases by 0.8 $^{\circ}\text{C}$ in IPSL-CM5A-LR and by 1.1 $^{\circ}\text{C}$ in bcc-csm1-1. Under RCP

340 4.5, temperature keeps increasing but in a slower rate than before 2100 (IPSL-CM5A-LR: 1.3°C vs. bcc-csm1-1: 0.4°C).
341 Meanwhile, precipitation slightly decreases under RCP 2.6 (IPSL-CM5A-LR: -12.0 mm·yr⁻¹ vs. bcc-csm1-1: -5.8 mm·yr⁻¹)
342 while increases under RCP 4.5 (IPSL-CM5A-LR: 29.1 mm·yr⁻¹ vs. bcc-csm1-1: 8.5 mm·yr⁻¹) (Figure 2-4.1(a-b) & 2(a-b), SI
343 Table 23). Different from RCP 2.6 and RCP 4.5, the increase in temperature and precipitation under RCP 8.5 is stable
344 ~~during throughout~~ 1990-22300, and slows down after 2200. In particular, under IPSL-CM5A-LR, during 1990-2100 and
345 2100-2300, temperature increases by 8.4 and 8.1 °C while precipitation increases by 106.1 and 131.7 mm·yr⁻¹. Under bcc-
346 csm1-1, during 1990-2100 and 2100-2300, temperature increases by 7.2 and 6.9 °C while precipitation increases by 100.9
347 and 198 mm·yr⁻¹, respectively (Figure 2-4.1(1-2)c, SI Table 23).

348 The result of pan-Arctic wetland shrinking under all scenarios indicates that the increase of precipitation does not
349 compensate the increase of evapotranspiration under warmer climate. Therefore, the pan-Arctic generally becomes drier and
350 WTD becomes deeper (Figure 2-4.3(a-c), SI Figure 6&7). In particular, during 1990-2100, under IPSL-CM5A-LR, wetland
351 shrinks by 0.6, 0.9 and 1.4 million km² under three RCP scenarios. Meanwhile, under bcc-csm1-1, wetland shrinks slightly
352 less by 0.4, 0.6 and 1.2 million km² under three RCP scenarios, respectively. During 2100-2300, under both IPSL-CM5A-LR
353 and bcc-csm1-1, wetlands slightly expand by 0.1 million km² under RCP 2.6, while under the warmer scenarios, wetland
354 further shrinks by 0.2 and 0.9 million km², respectively (Figure 2-4.3(a-c), SI Table 23).

355 Following climate warming, permafrost shrink is simulated across the current pan-Arctic peatland region under all
356 scenarios (Figure 2-4.4(a-c)). In particular, with IPSL-CM5A-LR forcing, under RCP 2.6, 4.5 and 8.5, permafrost shrinks by
357 0.2, 0.7 and 1.2 million km² during 1990-2100 and expands by 0.1, shrinks by 0.1 and 0.5 million km², respectively, during
358 2100-2300. Meanwhile, active layer deepening is simulated in the remaining permafrost region (SI Figure 86). Similarly,
359 with bcc-csm1-1 forcing, under RCP 2.6, 4.5 and 8.5, permafrost shrinks by 0.2, 0.2 and 1.0 million km² during 1990-2100
360 and expands by 0.1, shrinks by 0.1 and 0.6 million km², respectively, during 2100-2300 (Figure 2-4.4(a-c), SI Table 23).
361 Meanwhile, active layer deepening is simulated in the remaining permafrost region under RCP 4.5 and 8.5 (SI Figure 97).

362 Under RCP 2.6 and 4.5, with both IPSL-CM5A-LR and bcc-csm1-1 forcing, peatlands (i.e., the region with peat
363 thickness >= 30cm) area expands during 1990-2300 (Figure 53). In particular, the new peat area expands by 0.1 to 0.2
364 million km², while the old peat area is stable (SI Table 23). Under RCP 8.5, however, peatland area shrinks. In particular,
365 although new peat land area expands by 0.1 million km², the old peatland area shrinks by 0.1 to 0.4 million km², causing
366 total peatland area decrease (Figure 53, SI Table 23).



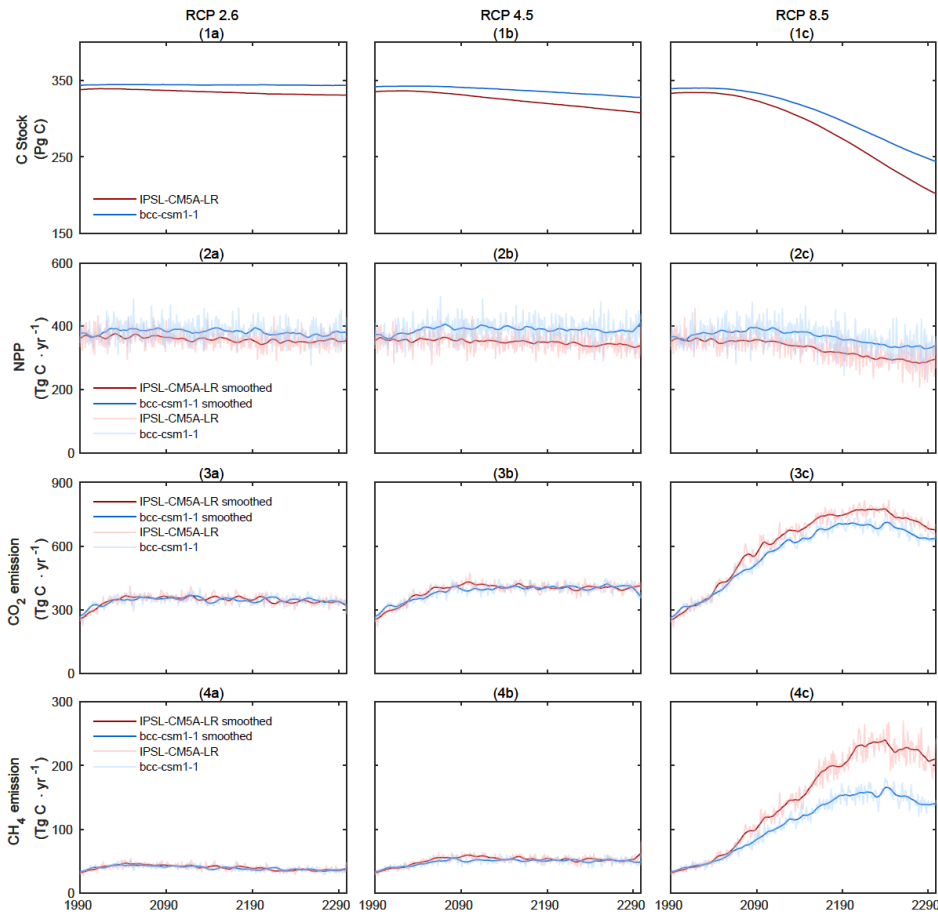
367
368 Figure 53. Time series of pan-Arctic old and new peatland area (million km²) during 1990-2300.

369 3.2 Pan-Arctic C stocks and fluxes under climate change

370 3.2.1 Before 2100

371 With WTD becomes deeper, active layer depth (ALD) becomes deeper and permafrost extent shrink, it is
 372 reasonable that decomposition increases during 1990-2100 under all scenarios (Figure 4-6_3&4 (a-c), SI-Table 23).
 373 Meanwhile, NPP slightly decreases with IPSL-CM5A-LR forcing while increases with bcc-csm1-1 forcing (Figure 4-6_2(a-
 374 c), SI-Table 23). In PTEM 2.2, NPP is primarily influenced by temperature and nitrogen availability, and available nitrogen
 375 mainly comes from net N mineralization. In all scenarios, net N mineralization rate increases (negative values indicate
 376 higher net N mineralization) during 1990-2100 (SI Figure 108), indicating more available N for vegetation. The increase in
 377 both N availability and temperature can not explain the reason for NPP decrease. However, NPP decrease can be explained
 378 by the shift in PFTs. In particular, during 1990-2100, with water table becomes deeper, the dominance of herbaceous plants
 379 is gradually replaced by woody plants (i.e., shrubs and trees) that can thrive under drier conditions (SI Figure 119). In PTEM
 380 2.2, compared with herbaceous plants, woody plants require more nitrogen for production. Therefore, although N availability
 381 increases, the increase is not sufficient for woody plants to maintain as high NPP as herbaceous plants and the overall NPP
 382 decreases.

383



384

385 **Figure 64.** Time series of pan-Arctic peatland C storage (vegetation and soil, Pg C), NPP ($\text{TgC}\cdot\text{yr}^{-1}$), CO_2 emissions from soil
 386 **heterotrophic respiration** ($\text{TgC}\cdot\text{yr}^{-1}$) and CH_4 emissions ($\text{TgC}\cdot\text{yr}^{-1}$) during 1990-2300.

387

388 In all scenarios except for bcc-csm1-1 RCP 2.6, the increase in decomposition overrides the increase in NPP and
 389 thereby C stock decreases (Figure 64 1(a-c), SI-Table 23). In particular, with ISP-CM5A-LR forcing, by 2100, C stock
 390 decreases by 1.3, 5.2 and 13.3 Pg C under RCP 2.6, 4.5 and 8.5, respectively. With bcc-csm1-1 forcing, by 2100, C stock
 391 increases by 0.8 Pg C under RCP 2.6, while decreases by 1.2 and 7.8 Pg C under RCP 4.5 and 8.5, respectively (Figure 64
 1(a-c), SI-Table 23). Notably, although pan-Arctic peatlands are C sinks during 1990-2100 under bcc-csm1-1 RCP 2.6, the

Formatted: Subscript

Formatted: Subscript

392 sink is much lower than that during 1940-1990 with CAR decreases by 29.1 gC·m⁻²·yr⁻¹. Furthermore, this difference is
 393 larger in the other scenarios (IPSL-CM5A-LR: 35.5-63.5 gC·m⁻²·yr⁻¹, bcc-csm1-1: 34.6-50.0 gC·m⁻²·yr⁻¹) (SI Figure
 394 120&134, SI-Table 34).

395 **Table 2. Pan-Arctic total C stock and annual C fluxes in 1990, 2100 and 2300**

		IPSL-CM5A-LR			bcc-csm1-1		
		RCP 2.6	RCP 4.5	RCP 8.5	RCP 2.6	RCP 4.5	RCP 8.5
C stock (Pg C)	1990	338.1	335.4	333.3	343.7	341.8	339.3
	2100	336.8	330.2	320.0	344.5	340.6	331.5
	2300	330.9	307.7	201.7	343.8	328.0	243.9
NPP (TgC·yr ⁻¹)	1990	362.2	355.0	352.4	377.6	373.1	366.2
	2100	361.4	348.2	350.9	390.7	391.5	387.7
	2300	354.4	340.0	297.5	381.4	413.2	339.0
CO ₂ emission (TgC·yr ⁻¹)	1990	257.9	254.3	252.5	272.2	269.2	265.8
	2100	357.0	430.1	618.5	352.7	389.9	558.0
	2300	320.0	413.5	676.1	321.1	359.5	636.5
CH ₄ emission (TgC·yr ⁻¹)	1990	31.8	31.7	31.7	33.8	33.7	33.7
	2100	42.4	59.2	118.8	42.3	49.5	92.9
	2300	37.9	62.9	210.7	37.9	48.5	140.5

396 * C stock includes both soil and vegetation C.

397

398 **Table 3. Pan-Arctic peatlands C accumulation rate during four time periods**

		IPSL-CM5A-LR			bcc-csm1-1		
		RCP 2.6	RCP 4.5	RCP 8.5	RCP 2.6	RCP 4.5	RCP 8.5
C accumulation rate (gC·m ⁻² ·yr ⁻¹)	1940-1990	32.5	31.9	31.8	32.1	32.1	31.5
	1990-2090	-3.0	-13.0	-33.5	3.0	-2.5	-18.5
	2090-2190	-12.3	-38.7	-169.0	-1.1	-18.2	-122.2
	2190-2290	-7.6	-36.9	-227.3	-1.9	-23.1	-163.8

399 * C accumulation rate is averaged from all grid cells weighted by the spatially-explicit peatland area.

400

401 3.2.2 During 2100-2300

402 During 2100-2300, the decrease in decomposition rate is simulated in RCP 2.6 and 4.5 with both forcing, while
 403 decomposition rate becomes higher under RCP 8.5 (SI-Table 23). Under RCP 2.6, the decrease in decomposition is driven by
 404 the colder and wetter climate (Figure 42), while with IPSL-CM5A-LR forcing the decrease of C stock also influences

Formatted: Indent: First line: 0"

Formatted: Font: 12 pt

Formatted: Font: 12 pt

Formatted

Formatted: Indent: First line: 0"

405 decomposition rate negatively. In contrast, under RCP 4.5 where climate becomes warmer and drier, the decrease in
406 decomposition rate is mostly driven by the lower C stock available for decomposition. However, under RCP 8.5 where the
407 climate change is more severe, the positive effect of warming and drying overrides the negative effect of insufficient C stock
408 and thereby decomposition rate keeps increasing (Figure 4_6_3&4(a-c), SI-Table 23).

409 During 2100-2300, NPP in all scenarios decrease except for bcc-csm1-1 RCP 4.5 (Figure 64 2(a-b), SI-Table 23).
410 For both forcings, under RCP 2.6 and 4.5, PFT distribution is stable after 2100 (SI Figure 119 1&2(a-b)). Therefore, NPP is
411 driven by the balance of net N mineralization and temperature. For bcc-csm1-1 RCP 4.5, the positive effect of temperature
412 overrides the negative effect of decreasing net N mineralization, while the opposite is found in the other scenarios (SI Figure
413 108). Under RCP 8.5, with further herbaceous-woody switch and decrease in net N mineralization, NPP decreases with both
414 forcings (Figure 64 2(c), SI-Table 23). With NPP decrease and decomposition increase, pan-Arctic peatlands are C sources
415 under all scenarios. In particular, with IPSL-CM5A-LR forcing, under RCP 2.6, 4.5 and 8.5, pan-Arctic peatlands are
416 sources of 5.9, 22.5 and 118.3 Pg C, respectively, while these values are 0.7, 12.6 and 87.6 Pg C with bcc-csm1-1 forcing,
417 respectively (Figure 64 1(a-c), SI-Table 23). During 2100-2300, CAR is lower than that during the 21st century. In
418 particular, under RCP 2.6, 4.5 and 8.5, CAR further decreases by 4.6-9.3 $\text{gC}\cdot\text{m}^{-2}\cdot\text{yr}^{-1}$, 23.9-25.7 $\text{gC}\cdot\text{m}^{-2}\cdot\text{yr}^{-1}$ and 135.5-193.8
419 $\text{gC}\cdot\text{m}^{-2}\cdot\text{yr}^{-1}$ with IPSL-CM5A-LR forcing and 4.1-4.9 $\text{gC}\cdot\text{m}^{-2}\cdot\text{yr}^{-1}$, 15.7-20.6 $\text{gC}\cdot\text{m}^{-2}\cdot\text{yr}^{-1}$ and 103.7-145.3 $\text{gC}\cdot\text{m}^{-2}\cdot\text{yr}^{-1}$ with
420 bcc-csm1-1 forcing, respectively (SI Figure 120&134, SI-Table 34).

421 3.3 Pan-Arctic peatlands C sinks in response to climate change

422 For both IPSL-CM5A-LR and bcc-csm1-1 forcings, the positive correlation between temperature and precipitation
423 is found at the pan-Arctic scale (Table 44). In particular, with 1°C annual temperature increase, the annual precipitation
424 increases by 13.84-15.33 $\text{mm}\cdot\text{yr}^{-1}$ in IPSL-CM5A-LR forcing and 13.78-14.59 $\text{mm}\cdot\text{yr}^{-1}$ in bcc-csm1-1 forcing. The
425 correlation has higher R^2 values in warmer scenarios. The positive correlation between temperature and precipitation is
426 mostly found in Eurasia and northeast America, where the R^2 values are also higher than the other region (SI Figure
427 142&153).

428 The negative correlation between temperature and pan-Arctic peatland C sink activity is found in both forcing
429 scenarios (Table 44). In particular, with 1°C annual temperature increase, pan-Arctic peatland C sink decreases by 40.46-
430 46.91 $\text{Tg C}\cdot\text{yr}^{-1}$ in IPSL-CM5A-LR forcing and 33.27-41.1 $\text{Tg C}\cdot\text{yr}^{-1}$ in bcc-csm1-1 forcing. The negative effect of
431 temperature is weaker in western Eurasia and Alaska regions, while stronger in the other regions where most of the current
432 peatlands exist (SI Figure 164&175). Due to the close positive correlation between temperature and precipitation, the
433 correlation between precipitation and pan-Arctic peatland C sink is also negative. In particular, with 1mm annual
434 precipitation increase, pan-Arctic peatland C sink decreases by 2.32-3.28 $\text{Tg C}\cdot\text{yr}^{-1}$ in IPSL-CM5A-LR forcing and 1.85-2.92
435 $\text{Tg C}\cdot\text{yr}^{-1}$ in bcc-csm1-1 forcing (Table 44). The spatial pattern of precipitation-C sink correlation is consistent with the
436 spatial pattern of temperature-C sink correlation (SI Figure 186&197).

437 At the pan-Arctic scale, a threshold annual temperature and precipitation can be found when peatlands switch from
438 a C sink to a source. In particular, with IPSL-CM5A-LR forcing, the threshold annual temperature is -2.89 - -2.6°C, the

439 [corresponding annual unfrozen day number is 169-180 days](#) and the threshold precipitation is 479.59 - 482.55 mm. With
 440 bcc-csm1-1 forcing, the threshold annual temperature is -2.35 - -2.09°C, [the corresponding annual unfrozen day number is](#)
 441 [176-181 days](#) and the threshold precipitation is 484.69 - 489.02 mm (Table 44). The threshold temperature varies spatially
 442 with mostly below -3°C in the northern North American and western Eurasia regions and mostly above 1°C in the lower
 443 latitude regions (SI Figure 2048). Notably, the regions with below -3°C threshold temperature tend to have higher R² values
 444 (SI Figure 2149). The spatial pattern of precipitation threshold is consistent with temperature threshold and the region with
 445 300-500mm annual precipitation threshold has higher R² values, mostly seen in northern North American and western
 446 Eurasia (SI Figure 220&231).

447 **Table 41.** Relationship between pan-Arctic temperature, precipitation and C sink

Model	RCP 2.6	R ²	RCP 4.5	R ²	RCP 8.5	R ²
Pan-Arctic peatlands C sink capability increases (TgC·yr ⁻¹) in response to 1°C annual temperature increase						
IPSL-CM5A-LR	-43.92	0.72	-40.46	0.86	-46.91	0.96
bcc-csm1-1	-34.59	0.51	-33.27	0.76	-41.1	0.96
Pan-Arctic peatlands C sink capability increases (TgC·yr ⁻¹) in response to 1mm annual precipitation increase						
IPSL-CM5A-LR	-2.32	0.64	-2.47	0.78	-3.28	0.92
bcc-csm1-1	-1.85	0.46	-2.06	0.73	-2.92	0.94
Annual temperature threshold of C sink-source conversion						
IPSL-CM5A-LR	-2.89 (180*)	0.57	-2.72 (179*)	0.9	-2.6 (169*)	0.86
bcc-csm1-1	-2.35 (181*)	0.16	-2.12 (184*)	0.64	-2.09 (176*)	0.81
Annual precipitation threshold of C sink-source conversion						
IPSL-CM5A-LR	479.59	0.51	482.42	0.86	482.55	0.84
bcc-csm1-1	489.02	0.16	485.5	0.63	484.69	0.79
Annual precipitation increase (mm) in response to 1°C annual temperature increase						
IPSL-CM5A-LR	15.33	0.74	14.71	0.9	13.84	0.98
bcc-csm1-1	13.78	0.61	14.59	0.85	13.78	0.98

448 * Values are the number of unfrozen days corresponding with the threshold temperature.

449 4. Discussion

450 4.1 Wetlands and permafrost dynamics under climate change

451 Wetlands loss is closely related to climate change and human activities. In particular, the loss has been found
 452 globally since 1700AD, with 64-71% loss since 1900 AD (Davidson, 2014). Similarly, a more recent study has found 33%
 453 of the global wetland loss as of 2009, with 45% in Europe and 8% in North America (Hu et al., 2017). In addition, regional
 454 studies also report different scales of wetlands loss in China and coastal regions (Li et al., 2018; Niu et al., 2012). To date,
 455 not many studies focus on future wetland extent simulations and the inconsistency among current wetland extent datasets

456 exists (Loveland et al., 2000; Friedl et al., 2002; Lehner and Döll, 2004; Bartholomé and Belward, 2005). Similar to this
457 study, one study highlighted the vulnerability of Arctic wetland extent in the 21st century due to permafrost thaw, although
458 most of the permafrost Arctic wetlands can remain stable under RCP 2.6 until at least 2100 (Kåresdotter et al., 2021).

459 The active layer depth-(ALD) simulated by PTEM 2.2 is compared with two datasets derived from satellite data and
460 models, covering pan-Arctic region and Alaska, respectively (Obu et al., 2020; Yi and Kimball, 2020). The correlation with
461 pan-Arctic dataset (2001-2018) is higher than the correlation with Alaska dataset, while the overall estimation is consistent
462 between our study and two regional datasets (SI-SI Table 43&54). Consistent with our study, Smith et al. (2022) found
463 deepening active layer depthALD since the 1990s in the permafrost region, indicating permafrost thaw could continue in
464 warmer future and possibly in a higher rate. The permafrost thaw progress in the 21st century agrees with the dynamics
465 simulated by CCSM4 model, suggesting that the CCSM4 permafrost area shrinks by 64% by 2100 under RCP 8.5 compared
466 to our estimation of 53-60% in this study (Lawrence et al., 2012).

467 **4.2 Future productivity and decomposition in northern peatlands**

468 In this study, NPP does not always increase under warmer climate due to PFT switch and net N mineralization rate
469 limiting. The overall trend of pan-Arctic peatland PFT switch is the expansion of woody plants and shrink of herbaceous
470 plants (SI Figure 119). A previous study found that peatland WTD deepening benefits shrub dominance while suppresses
471 forbs and mosses (Mäkiranata et al., 2018). Meanwhile, shrub expansion is reported in Alaska, Siberian and across the pan-
472 Arctic region under historical climate warming (Tape et al., 2006; Blok et al., 2010). Furthermore, the simulation based on
473 LPJ-GUESS also predicts higher proportion of shrub NPP in lower latitude regions due to high insolation and deep WTD
474 (Chaudhary et al., 2020). These studies support our findings that the future warmer and drier condition is the driver for PFT
475 switch and benefits woody plants. Notably, the fraction of woody plants could be overestimated because the PFTs in the
476 potential peatlands are included, where the WTD is usually lower than the existing peatlands and is more suitable for woody
477 plants (SI Figure 11). In the previous PTEM simulation for 15ka BP-1990, when these potential peatlands are not included
478 and WTD is not derived from TOPMODEL, the fraction of herbaceous plants is generally higher than the fraction in this
479 study (Zhao et al., 2022b).

480 In PTEM 2.2, the net N mineralization rate is related to soil moisture (Zhao et al., 2022b). Therefore, whether future
481 peatlands become more nutrient rich depends on the balance between the positive effect of higher temperature and the
482 negative effect of lower soil moisture. A site-level study on ombrotrophic bog has found increased plant available
483 ammonium under multi-year warming treatment (Iversen et al., 2022). The negative effect of drier soil overwhelms the
484 influence of temperature and thereby net N mineralization rate decrease under RCP 8.5 after 2100 (SI Figure 108). Under a
485 N limiting condition, the ~~modeling~~modelling study with LPX-Bern 1.0 found peatlands switch from a C sink to a source
486 under RCP 8.5 with slow NPP increase, which is consistent with our simulation with bcc-csm1-1 forcing (Spahni et al.,
487 2013).

488 Warming affects decomposition mainly in three ways. First, there is higher decomposition rate due to the lower
489 WTD under warming climate conditions (Huang et al., 2021). Second, higher temperature also enhances decomposition

490 more than productivity (Tang et al., 2022). Third, in high latitude regions, soil C decomposition rate is likely to increase
 491 under warmer climate and permafrost thaw conditions (Yokohata et al., 2020; Schneider Von Deimling et al., 2015; Gasser
 492 et al., 2018; Macdougall and Knutti, 2016; Schuur et al., 2015). In the warming future, the estimation of CO₂ release under
 493 RCP 2.6 tends to be higher than the values estimated from other models (by 2100: 54.7-54.8 Pg C in this study vs. 20-58 Pg
 494 C in literature; by 2300: 131.2-131.3 Pg C in this study vs. 40-98 Pg C in literature, Table 25). However, the estimation
 495 under RCP 8.5 is closer (by 2100: 55.2-57.2 Pg C in this study vs. 42-141 Pg C in literature; by 2300: 222.2-247.6 Pg C in
 496 this study vs. 157-313 Pg C in literature) (Yokohata et al., 2020; Schneider Von Deimling et al., 2015; Gasser et al., 2018)
 497 (Table 25). The CH₄ emission estimation is also higher than that in Yokohata (2020) by 5-6 Pg C by 2100, while the total C
 498 emission is close to the estimation of MacDougall (2016) (55 Pg C vs. 56 Pg C).

499 **Table 5.** Comparison of cumulative C emissions between this study and literature

<u>Emission source</u>	<u>Period</u>	<u>RCP scenario</u>	<u>C release</u>	<u>Region</u>	<u>Source</u>
<u>CO₂ (Pg C)</u>	<u>2100</u>	<u>RCP 2.6</u>	<u>54.7-54.8</u>	<u>pan-Arctic peatlands</u>	<u>This study</u>
			<u>21</u>	<u>permafrost region</u>	<u>Yokohata et al. (2020)</u>
			<u>20-58</u>	<u>permafrost region</u>	<u>Schneider Von Deimling et al. (2015)</u>
		<u>27</u>	<u>permafrost region</u>	<u>Gasser et al. (2018)</u>	
		<u>RCP 8.5</u>	<u>55.2-57.2</u>	<u>pan-Arctic peatlands</u>	<u>This study</u>
			<u>47</u>	<u>permafrost region</u>	<u>Yokohata et al. (2020)</u>
	<u>42-141</u>		<u>permafrost region</u>	<u>Schneider Von Deimling et al. (2015)</u>	
	<u>2300</u>	<u>RCP 2.6</u>	<u>59</u>	<u>permafrost region</u>	<u>Gasser et al. (2018)</u>
			<u>131.2-131.3</u>	<u>pan-Arctic peatlands</u>	<u>This study</u>
			<u>40-98</u>	<u>permafrost region</u>	<u>Schneider Von Deimling et al. (2015)</u>
		<u>RCP 8.5</u>	<u>47</u>	<u>permafrost region</u>	<u>Gasser et al. (2018)</u>
			<u>222.2-247.6</u>	<u>pan-Arctic peatlands</u>	<u>This study</u>
<u>157-313</u>			<u>permafrost region</u>	<u>Schneider Von Deimling et al. (2015)</u>	
<u>CH₄ (Pg C)</u>	<u>2100</u>	<u>RCP 2.6</u>	<u>212</u>	<u>permafrost region</u>	<u>Gasser et al. (2018)</u>
			<u>6</u>	<u>pan-Arctic peatlands</u>	<u>This study</u>
			<u>1</u>	<u>permafrost region</u>	<u>Yokohata et al. (2020)</u>
	<u>RCP 8.5</u>	<u>7.7-8.4</u>	<u>pan-Arctic peatlands</u>	<u>This study</u>	
		<u>1.5</u>	<u>permafrost region</u>	<u>Yokohata et al. (2020)</u>	
		<u>6</u>	<u>pan-Arctic peatlands</u>	<u>This study</u>	
<u>Total (Pg C)</u>	<u>2100</u>	<u>RCP 2.6</u>	<u>55</u>	<u>pan-Arctic peatlands</u>	<u>This study</u>
			<u>56</u>	<u>permafrost region</u>	<u>Macdougall and Knutti (2016)</u>
		<u>RCP 8.5</u>	<u>62.9-65.6</u>	<u>pan-Arctic peatlands</u>	<u>This study</u>
			<u>48</u>	<u>permafrost region</u>	<u>Yokohata et al. (2020)</u>
			<u>92 ± 17</u>	<u>permafrost region</u>	<u>Schneider Von Deimling et al. (2015)</u>
		<u>102</u>	<u>permafrost region</u>	<u>Macdougall and Knutti (2016)</u>	

Formatted: Font: 12 pt, Bold

Formatted: Font: 12 pt

Formatted Table

500

Formatted: Indent: Left: 0.44", First line: 0"

501 4.3 Northern peatland C sink and source shift

502 Our estimated CAR during 1990-2000 is 19.17-22.73 $\text{gC}\cdot\text{m}^{-2}\cdot\text{yr}^{-1}$, which is lower than that by Chaudhary et al.
503 (2020) during the same period (33.9 $\text{gC}\cdot\text{m}^{-2}\cdot\text{yr}^{-1}$). However, our estimated CAR is closer to the core-based Holocene CAR
504 (18.6-22.9 $\text{gC}\cdot\text{m}^{-2}\cdot\text{yr}^{-1}$) (Yu et al., 2009; Loisel et al., 2014). In this study, the estimated pan-Arctic peatlands annual CH_4
505 emissions are 28.7 $\text{Tg C}\cdot\text{yr}^{-1}$ during 1990-2000, 33.0 $\text{Tg C}\cdot\text{yr}^{-1}$ during 1990-2000 and 38.5 $\text{Tg C}\cdot\text{yr}^{-1}$ during 2000-2020. The
506 estimation after 1990 is close to the 36.0 $\text{Tg C}\cdot\text{yr}^{-1}$ in Kleinen et al. (2020) while larger than 25.0 $\text{Tg C}\cdot\text{yr}^{-1}$ reconstructed
507 from historical data (Treat et al., 2021). However, the difference between our study and Treat et al. (2021) might result from
508 different peatland coverages used in two studies. Under the peatland coverage of Nichols and Peteet (2019), the CH_4
509 emissions in Treat et al. (2021) were 32.3-43.5 $\text{Tg C}\cdot\text{yr}^{-1}$, which agrees better with our estimates.

510 Multiple studies have indicated there is a C loss trend of northern ecosystems under warming climate (Hanson et al.,
511 2020; Piao et al., 2008; Helbig et al., 2017). In particular, the peatland experiment in Minnesota, USA suggests that each 1°C
512 of warming increases C loss rate by 31.3 $\text{gC}\cdot\text{m}^{-2}\cdot\text{yr}^{-1}$ (Hanson et al., 2020). Similarly, another site-level study on Canadian
513 boreal-wetland biome shows a decline of CO_2 uptake from 25 ± 14 $\text{gC}\cdot\text{m}^{-2}\cdot\text{yr}^{-1}$ to 103 ± 38 $\text{gC}\cdot\text{m}^{-2}\cdot\text{yr}^{-1}$ by 2100 depending on
514 the warming scenarios (Helbig et al., 2017). These studies are consistent with our estimates, suggesting that northern
515 peatlands CAR during 1990-2100 is lower than that during 1940-1990 by 29.1-63.5 $\text{gC}\cdot\text{m}^{-2}\cdot\text{yr}^{-1}$.

516 At the regional scale, whether northern peatlands will switch from a C sink to C source is still uncertain. For
517 example, Gallego-Sala et al. (2018) indicates northern peatlands are likely to sequester more C under RCP 2.6 and RCP 8.5
518 until 2100. Chaudhary et al. (2020), however, indicates the C sink capacity of northern peatlands will decrease under RCP
519 8.5 after 2050. Similarly, McGuire et al. (2018) suggests northern permafrost region could be C sources after 2100 unless
520 under aggressive climate change mitigation pathways. Furthermore, Qiu et al. (2022) simulates northern peatlands dynamics
521 until 2300, suggesting a sink-source shift under RCP 8.5 while no such shift under RCP 2.6. Although conclusions vary
522 among studies, they generally suggest a higher C source possibility under warmer scenarios, which agrees with the negative
523 correlation between temperature and C sink capacity from this study. Furthermore, the arguments that northern peatlands
524 keep being C sinks under RCP 2.6 (Gallego-Sala et al., 2018; Qiu et al., 2022) is consistent with our study under bcc-csm1-1
525 forcing. However, different from previous works (Gallego-Sala et al., 2018; Qiu et al., 2022; McGuire et al., 2018;
526 Chaudhary et al., 2020), our study predicts northern peatlands to be C sources under RCP 2.6 before 2100 with IPSL-CM5A-
527 LR forcing. In addition, the C sink-source switch will occur before 2100 under RCP 4.5 and RCP 8.5. Except for the future
528 decomposition increase, which is common among model predictions (Yokohata et al., 2020; Schneider Von Deimling et al.,
529 2015; Gasser et al., 2018; Macdougall and Knutti, 2016; Schuur et al., 2015), these differences are mainly due to the
530 suppressed NPP in this study.

531 5. Conclusions

532 Northern peatlands responses to future climate change during 1990-2300 are simulated with PTEM. The peatlands
533 shrink or expansion, peat accumulation and decomposition processes are considered. Two sets of CMIP5 forcing data (IPSL-
534 CM5A-LR and bcc-csm1-1) are used to drive the model with three warming scenarios (RCP 2.6, RCP 4.5 and RCP 8.5). We
535 found that wetlands will shrink and permafrost will thaw under all scenarios, indicating pan-Arctic peatlands become

Formatted: Subscript

536 warmer and drier. Northern peatland area expands under RCP 2.6 and RCP 4.5 while shrinks under RCP 8.5 due to [the](#)
537 [shrinkage of the area with over 30cm peat thickness under](#) high decomposition rate. NPP does not always increase with
538 temperature because of PFT switch and N limiting effects. However, both CO₂ and CH₄ emissions increase with temperature
539 due to lower WTD, thawing permafrost and higher temperature. By 2100, northern peatlands will be a minor C sink of 0.8
540 Pg C under RCP 2.6 with bcc-csm1-1 forcing while C sources under other scenarios. During 2100-2300, northern peatlands
541 are C sources under all scenarios, the warmer climate results in the larger C source. There are negative correlations between
542 temperature and northern peatland C sink under all scenarios. The negative correlation between precipitation and northern
543 peatland C sink is also found under all scenarios, while this is likely due to the positive correlation between temperature and
544 precipitation. When pan-Arctic annual temperature is -2.89 - -2.6°C with IPSL-CM5A-LR forcing or -2.35 - -2.09°C with
545 bcc-csm1-1 forcing, the northern peatlands switch from a C sink to a source. Similarly, this threshold for annual precipitation
546 is 479.59 - 482.55 mm with IPSL-CM5A-LR forcing and 484.69 - 489.02 mm with bcc-csm1-1 forcing. Our study highlights
547 the current northern peatlands C sink might shift to a source under future warming and drying climate conditions.

548 Acknowledgments

549 This study is financially supported by an NSF project (1802832).

550 Coda and data availability:

551 The data used to reproduce figures in both text and supplementary material, PTEM 2.2 codes, model and samples of running
552 directory can be accessed via Purdue University Research Repository: <https://purr.purdue.edu/publications/4139/1>.

553 References

- 554 [Allen, M. R., Dube, O. P., Solecki, W., Aragón-Durand, F., W. Cramer, S. H., Kainuma, M., J. Kala, N. M., Mulugetta, Y.,](#)
555 [Perez, R., Wairiu, M., and Ziekfeld, K.: Framing and Context. In: Global Warming of 1.5°C. An IPCC Special Report](#)
556 [on the impacts of global warming of 1.5°C above pre-industrial levels and related global greenhouse gas emission](#)
557 [pathways, in the context of strengthening the global response to the threat of climate change, sustainable development,](#)
558 [and efforts to eradicate poverty, IPCC, 2018.](#)
- 559 Allen, R. G., Pereira, L. S., Raes, D., and Smith, M.: Crop evapotranspiration - Guidelines for computing crop water
560 requirements - FAO Irrigation and drainage paper 56, 1998.
- 561 Bartholomé, E. and Belward, A. S.: GLC2000: a new approach to global land cover mapping from Earth observation data,
562 International Journal of Remote Sensing, 26, 1959-1977, 10.1080/01431160412331291297, 2005.
- 563 Beven, K. J. and Kirkby, M. J.: A physically based, variable contributing area model of basin hydrology / Un modèle à base
564 physique de zone d'appel variable de l'hydrologie du bassin versant, Hydrological Sciences Bulletin, 24, 43-69,
565 10.1080/02626667909491834, 1979.
- 566 Blok, D., Heijmans, M. M. P. D., Schaepe-man-Strub, G., Kononov, A. V., Maximov, T. C., and Berendse, F.: Shrub
567 expansion may reduce summer permafrost thaw in Siberian tundra, Global Change Biology, 16, 1296-1305,
568 <https://doi.org/10.1111/j.1365-2486.2009.02110.x>, 2010.
- 569 Bohn, T. J., Podest, E., Schroeder, R., Pinto, N., McDonald, K. C., Glagolev, M., Filippov, I., Maksyutov, S., Heimann, M.,
570 Chen, X., and Lettenmaier, D. P.: Modeling the large-scale effects of surface moisture heterogeneity on wetland carbon
571 fluxes in the West Siberian Lowland, Biogeosciences, 10, 6559-6576, 10.5194/bg-10-6559-2013, 2013.
- 572 Brooks, R. H.: HYDRAULIC PROPERTIES OF POROUS MEDIA, Ph.D., Colorado State University, Ann Arbor, 101 pp.,
573 1965.
- 574 Carter, A. J. and Scholes, R. J.: SoilData v2.0: Generating a Global Database of Soil Properties CSIR Environmentek,
575 Pretoria, South Africa, 2000.

576 Chaudhary, N., Miller, P. A., and Smith, B.: Modelling past, present and future peatland carbon accumulation across the pan-
577 Arctic region, *Biogeosciences*, 14, 4023-4044, 10.5194/bg-14-4023-2017, 2017.

578 Chaudhary, N., Westermann, S., Lamba, S., Shurpali, N., Sannel, A. B. K., Schurgers, G., Miller, P. A., and Smith, B.:
579 Modelling past and future peatland carbon dynamics across the pan-Arctic, *Global Change Biology*, n/a,
580 10.1111/gcb.15099, 2020.

581 Davidson, N. C.: How much wetland has the world lost? Long-term and recent trends in global wetland area, *Marine and*
582 *Freshwater Research*, 65, 934-941, <https://doi.org/10.1071/MF14173>, 2014.

583 Fan, Y., Li, H., and Miguez-Macho, G.: Global Patterns of Groundwater Table Depth, *Science*, 339, 940,
584 10.1126/science.1229881, 2013.

585 FAO/UNESCO: Soil Map of the World, Food and Agriculture Organization of the United Nations, Paris, 1974.

586 Finger Higgens, R. A., Chipman, J. W., Lutz, D. A., Culler, L. E., Virginia, R. A., and Ogden, L. A.: Changing Lake
587 Dynamics Indicate a Drier Arctic in Western Greenland, *Journal of Geophysical Research: Biogeosciences*, 124, 870-
588 883, <https://doi.org/10.1029/2018JG004879>, 2019.

589 Finlayson, C. M. and Milton, G. R.: Peatlands, in: *The Wetland Book: II: Distribution, Description, and Conservation*, edited
590 by: Finlayson, C. M., Milton, G. R., Prentice, R. C., and Davidson, N. C., Springer Netherlands, Dordrecht, 227-244,
591 10.1007/978-94-007-4001-3_202, 2018.

592 Franchini, M. and Pacciani, M.: Comparative analysis of several conceptual rainfall-runoff models, *Journal of Hydrology*,
593 122, 161-219, [https://doi.org/10.1016/0022-1694\(91\)90178-K](https://doi.org/10.1016/0022-1694(91)90178-K), 1991.

594 Friedl, M. A., McIver, D. K., Hodges, J. C. F., Zhang, X. Y., Muchoney, D., Strahler, A. H., Woodcock, C. E., Gopal, S.,
595 Schneider, A., Cooper, A., Baccini, A., Gao, F., and Schaaf, C.: Global land cover mapping from MODIS: algorithms
596 and early results, *Remote Sensing of Environment*, 83, 287-302, [https://doi.org/10.1016/S0034-4257\(02\)00078-0](https://doi.org/10.1016/S0034-4257(02)00078-0), 2002.

597 Gallego-Sala, A. V., Charman, D. J., Brewer, S., Page, S. E., Prentice, I. C., Friedlingstein, P., Moreton, S., Amesbury, M. J.,
598 Beilman, D. W., Björck, S., Blyakharchuk, T., Bochicchio, C., Booth, R. K., Bunbury, J., Camill, P., Carless, D.,
599 Chimner, R. A., Clifford, M., Cressey, E., Courtney-Mustaphi, C., De Vleeschouwer, F., de Jong, R., Fialkiewicz-
600 Koziel, B., Finkelstein, S. A., Garneau, M., Githumbi, E., Hribljan, J., Holmquist, J., Hughes, P. D. M., Jones, C., Jones,
601 M. C., Karofeld, E., Klein, E. S., Kockfelt, U., Korhola, A., Lacourse, T., Le Roux, G., Lamentowicz, M., Large, D.,
602 Lavoie, M., Loisel, J., Mackay, H., MacDonald, G. M., Makila, M., Magnan, G., Marchant, R., Marcisz, K., Martínez
603 Cortizas, A., Massa, C., Mathijssen, P., Mauquoy, D., Mighall, T., Mitchell, F. J. G., Moss, P., Nichols, J., Oksanen, P.
604 O., Orme, L., Packalen, M. S., Robinson, S., Roland, T. P., Sanderson, N. K., Sannel, A. B. K., Silva-Sánchez, N.,
605 Steinberg, N., Swindles, G. T., Turner, T. E., Uglow, J., Väliranta, M., van Bellen, S., van der Linden, M., van Geel, B.,
606 Wang, G., Yu, Z., Zaragoza-Castells, J., and Zhao, Y.: Latitudinal limits to the predicted increase of the peatland carbon
607 sink with warming, *Nature Climate Change*, 8, 907-913, 10.1038/s41558-018-0271-1, 2018.

608 Gandois, L., Hoyt, A. M., Hatté, C., Jeanneau, L., Teisserenc, R., Liotaud, M., and Tananaev, N.: Contribution of Peatland
609 Permafrost to Dissolved Organic Matter along a Thaw Gradient in North Siberia, *Environmental Science & Technology*,
610 53, 14165-14174, 10.1021/acs.est.9b03735, 2019.

611 Gasser, T., Kechiar, M., Ciais, P., Burke, E. J., Kleinen, T., Zhu, D., Huang, Y., Ekici, A., and Obersteiner, M.: Path-
612 dependent reductions in CO₂ emission budgets caused by permafrost carbon release, *Nature Geoscience*, 11, 830-835,
613 10.1038/s41561-018-0227-0, 2018.

614 **GISTEMP-Team: GISS Surface Temperature Analysis (GISTEMP), version 4, NASA Goddard Institute for Space Studies**
615 **[dataset], 2021.**

616 Hamman, J. J., Nijssen, B., Bohn, T. J., Gergel, D. R., and Mao, Y.: The Variable Infiltration Capacity model version 5
617 (VIC-5): infrastructure improvements for new applications and reproducibility, *Geosci. Model Dev.*, 11, 3481-3496,
618 10.5194/gmd-11-3481-2018, 2018.

619 Hanson, P. J., Griffiths, N. A., Iversen, C. M., Norby, R. J., Sebestyen, S. D., Phillips, J. R., Chanton, J. P., Kolka, R. K.,
620 Malhotra, A., Oleheiser, K. C., Warren, J. M., Shi, X., Yang, X., Mao, J., and Ricciuto, D. M.: Rapid Net Carbon Loss
621 From a Whole-Ecosystem Warmed Peatland, *AGU Advances*, 1, e2020AV000163,
622 <https://doi.org/10.1029/2020AV000163>, 2020.

623 Harris, I., Jones, P. D., Osborn, T. J., and Lister, D. H.: Updated high-resolution grids of monthly climatic observations – the
624 CRU TS3.10 Dataset, *International Journal of Climatology*, 34, 623-642, <https://doi.org/10.1002/joc.3711>, 2014.

625 He, F.: SIMULATING TRANSIENT CLIMATE EVOLUTION OF THE LAST DEGLACIATION WITH CCSM3,
626 Atmospheric and Oceanic Sciences, UNIVERSITY OF WISCONSIN-MADISON, Madison, 2011.

627 Helbig, M., Chasmer, L. E., Desai, A. R., Kljun, N., Quinton, W. L., and Sonntag, O.: Direct and indirect climate change
628 effects on carbon dioxide fluxes in a thawing boreal forest–wetland landscape, *Global Change Biology*, 23, 3231-3248,
629 <https://doi.org/10.1111/gcb.13638>, 2017.

630 Hu, S., Niu, Z., Chen, Y., Li, L., and Zhang, H.: Global wetlands: Potential distribution, wetland loss, and status, *Science of*
631 *The Total Environment*, 586, 319-327, <https://doi.org/10.1016/j.scitotenv.2017.02.001>, 2017.

632 Huang, Y., Ciais, P., Luo, Y., Zhu, D., Wang, Y., Qiu, C., Goll, D. S., Guenet, B., Makowski, D., De Graaf, I., Leifeld, J.,
633 Kwon, M. J., Hu, J., and Qu, L.: Tradeoff of CO2 and CH4 emissions from global peatlands under water-table
634 drawdown, *Nature Climate Change*, 11, 618-622, 10.1038/s41558-021-01059-w, 2021.

635 Hugelius, G., Loisel, J., Chadburn, S., Jackson, R. B., Jones, M., MacDonald, G., Marushchak, M., Olefeldt, D., Packalen,
636 M., Siewert, M. B., Treat, C., Turetsky, M., Voigt, C., and Yu, Z.: Large stocks of peatland carbon and nitrogen are
637 vulnerable to permafrost thaw, *Proceedings of the National Academy of Sciences*, 117, 20438,
638 10.1073/pnas.1916387117, 2020.

639 Hugelius, G., Bockheim, J. G., Camill, P., Elberling, B., Grosse, G., Harden, J. W., Johnson, K., Jorgenson, T., Koven, C. D.,
640 Kuhry, P., Michaelson, G., Mishra, U., Palmtag, J., Ping, C. L., O'Donnell, J., Schirrmeister, L., Schuur, E. A. G.,
641 Sheng, Y., Smith, L. C., Strauss, J., and Yu, Z.: A new data set for estimating organic carbon storage to 3 m depth in
642 soils of the northern circumpolar permafrost region, *Earth Syst. Sci. Data*, 5, 393-402, 10.5194/essd-5-393-2013, 2013.

643 [Iversen, C. M., Latimer, J., Brice, D. J., Childs, J., Vander Stel, H. M., Defrenne, C. E., Graham, J., Griffiths, N. A.,](#)
644 [Malhotra, A., Norby, R. J., Oleheiser, K. C., Phillips, J. R., Salmon, V. G., Sebestyen, S. D., Yang, X., and Hanson, P.](#)
645 [J.: Whole-Ecosystem Warming Increases Plant-Available Nitrogen and Phosphorus in an Ombrotrophic Bog,](#)
646 [Ecosystems](#), 10.1007/s10021-022-00744-x, 2022.

647 Kåresdotter, E., Destouni, G., Ghajarnia, N., Hugelius, G., and Kalantari, Z.: Mapping the Vulnerability of Arctic Wetlands
648 to Global Warming, *Earth's Future*, 9, e2020EF001858, <https://doi.org/10.1029/2020EF001858>, 2021.

649 Kleinen, T., Mikolajewicz, U., and Brovkin, V.: Terrestrial methane emissions from the Last Glacial Maximum to the
650 preindustrial period, *Clim. Past*, 16, 575-595, 10.5194/cp-16-575-2020, 2020.

651 Lawrence, D. M., Slater, A. G., and Swenson, S. C.: Simulation of Present-Day and Future Permafrost and Seasonally
652 Frozen Ground Conditions in CCSM4, *Journal of Climate*, 25, 2207-2225, 10.1175/JCLI-D-11-00334.1, 2012.

653 Lehner, B. and Döll, P.: Development and validation of a global database of lakes, reservoirs and wetlands, *Journal of*
654 *Hydrology*, 296, 1-22, <https://doi.org/10.1016/j.jhydrol.2004.03.028>, 2004.

655 Li, X., Bellerby, R., Craft, C., and Widney, S. E.: Coastal wetland loss, consequences, and challenges for restoration,
656 *Anthropocene Coasts*, 1, 1-15, 10.1139/anc-2017-0001, 2018.

657 Liang, X., Lettenmaier, D. P., Wood, E. F., and Burges, S. J.: A simple hydrologically based model of land surface water and
658 energy fluxes for general circulation models, *Journal of Geophysical Research: Atmospheres*, 99, 14415-14428,
659 <https://doi.org/10.1029/94JD00483>, 1994.

660 Liu, C., Sun, G., McNulty, S. G., Noormets, A., and Fang, Y.: Environmental controls on seasonal ecosystem
661 evapotranspiration/potential evapotranspiration ratio as determined by the global eddy flux measurements, *Hydrol.*
662 *Earth Syst. Sci.*, 21, 311-322, 10.5194/hess-21-311-2017, 2017.

663 Loisel, J., Yu, Z., Beilman, D. W., Camill, P., Alm, J., Amesbury, M. J., Anderson, D., Andersson, S., Bochicchio, C.,
664 Barber, K., Belyea, L. R., Bunbury, J., Chambers, F. M., Charman, D. J., De Vleeschouwer, F., Fiałkiewicz-Kozieł, B.,
665 Finkelstein, S. A., Galka, M., Garneau, M., Hammarlund, D., Hinchcliffe, W., Holmquist, J., Hughes, P., Jones, M. C.,
666 Klein, E. S., Kokfelt, U., Korhola, A., Kuhry, P., Lamarre, A., Lamentowicz, M., Large, D., Lavoie, M., MacDonald, G.,
667 Magnan, G., Mäkilä, M., Mallon, G., Mathijssen, P., Mauquoy, D., McCarroll, J., Moore, T. R., Nichols, J., O'Reilly,
668 B., Oksanen, P., Packalen, M., Peteet, D., Richard, P. J. H., Robinson, S., Ronkainen, T., Rundgren, M., Sannel, A. B.
669 K., Tarnocai, C., Thom, T., Tuittila, E.-S., Turetsky, M., Väiranta, M., van der Linden, M., van Geel, B., van Bellen, S.,
670 Vitt, D., Zhao, Y., and Zhou, W.: A database and synthesis of northern peatland soil properties and Holocene carbon
671 and nitrogen accumulation. *The Holocene*, 24, 1028-1042, 10.1177/0959683614538073, 2014.

672 Loisel, J., Gallego-Sala, A. V., Amesbury, M. J., Magnan, G., Anshari, G., Beilman, D. W., Benavides, J. C., Blewett, J.,
673 Camill, P., Charman, D. J., Chawchai, S., Hedgpeth, A., Kleinen, T., Korhola, A., Large, D., Mansilla, C. A., Müller, J.,
674 van Bellen, S., West, J. B., Yu, Z., Bubier, J. L., Garneau, M., Moore, T., Sannel, A. B. K., Page, S., Väiranta, M.,

675 Bechtold, M., Brovkin, V., Cole, L. E. S., Chanton, J. P., Christensen, T. R., Davies, M. A., De Vleeschouwer, F.,
676 Finkelstein, S. A., Frolking, S., Gałka, M., Gandois, L., Girkin, N., Harris, L. L., Heinemeyer, A., Hoyt, A. M., Jones, M.
677 C., Joos, F., Juutinen, S., Kaiser, K., Lacourse, T., Lamentowicz, M., Larmola, T., Leifeld, J., Lohila, A., Milner, A. M.,
678 Minkinen, K., Moss, P., Naafs, B. D. A., Nichols, J., O'Donnell, J., Payne, R., Philben, M., Piilo, S., Quillet, A.,
679 Ratnayake, A. S., Roland, T. P., Sjögersten, S., Sonntag, O., Swindles, G. T., Swinnen, W., Talbot, J., Treat, C.,
680 Valach, A. C., and Wu, J.: Expert assessment of future vulnerability of the global peatland carbon sink, *Nature Climate*
681 *Change*, 11, 70-77, 10.1038/s41558-020-00944-0, 2021.

682 Loveland, T. R., Reed, B. C., Brown, J. F., Ohlen, D. O., Zhu, Z., Yang, L., and Merchant, J. W.: Development of a global
683 land cover characteristics database and IGBP DISCover from 1 km AVHRR data, *International Journal of Remote*
684 *Sensing*, 21, 1303-1330, 10.1080/014311600210191, 2000.

685 Lu, X. and Zhuang, Q.: Modeling methane emissions from the Alaskan Yukon River basin, 1986–2005, by coupling a large-
686 scale hydrological model and a process-based methane model, *Journal of Geophysical Research: Biogeosciences*, 117,
687 <https://doi.org/10.1029/2011JG001843>, 2012.

688 MacDougall, A. H. and Knutti, R.: Projecting the release of carbon from permafrost soils using a perturbed parameter
689 ensemble modelling approach, *Biogeosciences*, 13, 2123-2136, 10.5194/bg-13-2123-2016, 2016.

690 Mäkiranta, P., Laiho, R., Mehtätalo, L., Straková, P., Sormunen, J., Minkinen, K., Penttilä, T., Fritze, H., and Tuittila, E.:
691 Responses of phenology and biomass production of boreal fens to climate warming under different water-table level
692 regimes, *Glob Chang Biol*, 24, 944-956, doi: 10.1111/gcb.13934, 2018.

693 Marthews, T. R., Dadson, S. J., Lehner, B., Abele, S., and Gedney, N.: High-resolution global topographic index values for
694 use in large-scale hydrological modelling, *Hydrol. Earth Syst. Sci.*, 19, 91-104, 10.5194/hess-19-91-2015, 2015.

695 McGuire, A. D., Lawrence, D. M., Koven, C., Clein, J. S., Burke, E., Chen, G., Jafarov, E., MacDougall, A. H., Marchenko,
696 S., Nicolsky, D., Peng, S., Rinke, A., Ciais, P., Gouttevin, I., Hayes, D. J., Ji, D., Krinner, G., Moore, J. C.,
697 Romanovsky, V., Schädel, C., Schaefer, K., Schuur, E. A. G., and Zhuang, Q.: Dependence of the evolution of carbon
698 dynamics in the northern permafrost region on the trajectory of climate change, *Proceedings of the National Academy*
699 *of Sciences*, 115, 3882, 10.1073/pnas.1719903115, 2018.

700 Meinshausen, M., Smith, S. J., Calvin, K., Daniel, J. S., Kainuma, M. L. T., Lamarque, J. F., Matsumoto, K., Montzka, S. A.,
701 Raper, S. C. B., Riahi, K., Thomson, A., Velders, G. J. M., and van Vuuren, D. P. P.: The RCP greenhouse gas
702 concentrations and their extensions from 1765 to 2300, *Climatic Change*, 109, 213, 10.1007/s10584-011-0156-z, 2011.

703 Melton, J. R., Chan, E., Millard, K., Fortier, M., Winton, R. S., Martín-López, J. M., Cadillo-Quiroz, H., Kidd, D., and
704 Verchot, L. V.: A map of global peatland extent created using machine learning (Peat-ML), *Geosci. Model Dev.*
705 *Discuss.*, 2022, 1-44, 10.5194/gmd-2021-426, 2022.

706 Miao, C., Duan, Q., Sun, Q., Huang, Y., Kong, D., Yang, T., Ye, A., Di, Z., and Gong, W.: Assessment of CMIP5 climate
707 models and projected temperature changes over Northern Eurasia, *Environmental Research Letters*, 9, 055007,
708 10.1088/1748-9326/9/5/055007, 2014.

709 Müller, J. and Joos, F.: Committed and projected future changes in global peatlands – continued transient model simulations
710 since the Last Glacial Maximum, *Biogeosciences*, 18, 3657-3687, 10.5194/bg-18-3657-2021, 2021.

711 Nichols, J. E. and Peteet, D. M.: Rapid expansion of northern peatlands and doubled estimate of carbon storage, *Nature*
712 *Geoscience*, 12, 917-921, 10.1038/s41561-019-0454-z, 2019.

713 Niu, Z., Zhang, H., Wang, X., Yao, W., Zhou, D., Zhao, K., Zhao, H., Li, N., Huang, H., Li, C., Yang, J., Liu, C., Liu, S.,
714 Wang, L., Li, Z., Yang, Z., Qiao, F., Zheng, Y., Chen, Y., Sheng, Y., Gao, X., Zhu, W., Wang, W., Wang, H., Weng, Y.,
715 Zhuang, D., Liu, J., Luo, Z., Cheng, X., Guo, Z., and Gong, P.: Mapping wetland changes in China between 1978 and
716 2008, *Chinese Science Bulletin*, 57, 2813-2823, 10.1007/s11434-012-5093-3, 2012.

717 Obu, J., Westermann, S., Barboux, C., Bartsch, A., Delaloye, R., Grosse, G., Heim, B., Hugelius, G., Irrgang, A., Kääb, A.
718 M., Kroisleitner, C., Matthes, H., Nitze, I., Pellet, C., Seifert, F. M., Strozzi, T., Wegmüller, U., Wieczorek, M., and
719 Wiesmann, A.: ESA Permafrost Climate Change Initiative (Permafrost_cci): Permafrost Climate Research Data
720 Package v1., Centre for Environmental Data Analysis [dataset],
721 <https://catalogue.ceda.ac.uk/uuid/1f88068e86304b0fbd34456115b6606f>, 2020.

722 Olefeldt, D., Hovemyr, M., Kuhn, M. A., Bastviken, D., Bohn, T. J., Connolly, J., Crill, P., Euskirchen, E. S., Finkelstein, S.
723 A., Genet, H., Grosse, G., Harris, L. I., Heffernan, L., Helbig, M., Hugelius, G., Hutchins, R., Juutinen, S., Lara, M. J.,
724 Malhotra, A., Manies, K., McGuire, A. D., Natali, S. M., O'Donnell, J. A., Parmentier, F. J. W., Räsänen, A., Schädel,

725 [C., Sonnentag, O., Strack, M., Tank, S. E., Treat, C., Varner, R. K., Virtanen, T., Warren, R. K., and Watts, J. D.: The](#)
726 [Boreal–Arctic Wetland and Lake Dataset \(BAWLD\). Earth Syst. Sci. Data, 13, 5127–5149, 10.5194/essd-13-5127-2021,](#)
727 [2021.](#)

728 Palmer, M. D., Harris, G. R., and Gregory, J. M.: Extending CMIP5 projections of global mean temperature change and sea
729 level rise due to thermal expansion using a physically-based emulator, *Environmental Research Letters*, 13, 084003,
730 10.1088/1748-9326/aad2e4, 2018.

731 Piao, S., Ciais, P., Friedlingstein, P., Peylin, P., Reichstein, M., Luysaert, S., Margolis, H., Fang, J., Barr, A., Chen, A.,
732 Grelle, A., Hollinger, D. Y., Laurila, T., Lindroth, A., Richardson, A. D., and Vesala, T.: Net carbon dioxide losses of
733 northern ecosystems in response to autumn warming, *Nature*, 451, 49–52, 10.1038/nature06444, 2008.

734 Qiu, C., Zhu, D., Ciais, P., Guenet, B., and Peng, S.: The role of northern peatlands in the global carbon cycle for the 21st
735 century, *Global Ecology and Biogeography*, 29, 956–973, <https://doi.org/10.1111/geb.13081>, 2020.

736 Qiu, C., Zhu, D., Ciais, P., Guenet, B., Peng, S., Krinner, G., Tootchi, A., Ducharme, A., and Hastie, A.: Modelling northern
737 peatland area and carbon dynamics since the Holocene with the ORCHIDEE-PEAT land surface model (SVN r5488),
738 *Geosci. Model Dev.*, 12, 2961–2982, 10.5194/gmd-12-2961-2019, 2019.

739 Qiu, C., Ciais, P., Zhu, D., Guenet, B., Chang, J., Chaudhary, N., Kleinen, T., Li, X., Müller, J., Xi, Y., Zhang, W.,
740 Ballantyne, A., Brewer, S. C., Brovkin, V., Charman, D. J., Gustafson, A., Gallego-Sala, A. V., Gasser, T., Holden, J.,
741 Joos, F., Kwon, M. J., Lauerwald, R., Miller, P. A., Peng, S., Page, S., Smith, B., Stocker, B. D., Sannel, A. B. K.,
742 Salmon, E., Schurgers, G., Shurpali, N. J., Wärlind, D., and Westermann, S.: A strong mitigation scenario maintains
743 climate neutrality of northern peatlands, *One Earth*, <https://doi.org/10.1016/j.oneear.2021.12.008>, 2022.

744 Rawls, W. J., Ahuja, L. R., Brakensiek, D. L., and Shirmohammadi, A.: Infiltration and soil water movement, in, McGraw-
745 Hill Inc., New York, 5.1–5.51, 1992.

746 [Richardson, A. D., Hufkens, K., Milliman, T., Aubrecht, D. M., Furze, M. E., Seyednasrollah, B., Krassovski, M. B.,](#)
747 [Latimer, J. M., Nettles, W. R., Heiderman, R. R., Warren, J. M., and Hanson, P. J.: Ecosystem warming extends](#)
748 [vegetation activity but heightens vulnerability to cold temperatures, Nature, 560, 368–371, 10.1038/s41586-018-0399-1,](#)
749 [2018.](#)

750 Schaperow, J. and Li, D.: VICGlobal: soil and vegetation parameters for the Variable Infiltration Capacity hydrological
751 model (1.6d) [dataset], <https://doi.org/10.5281/zenodo.5038653>, 2021.

752 Schneider von Deimling, T., Grosse, G., Strauss, J., Schirmer, L., Morgenstern, A., Schaphoff, S., Meinshausen, M., and
753 Boike, J.: Observation-based modelling of permafrost carbon fluxes with accounting for deep carbon deposits and
754 thermokarst activity, *Biogeosciences*, 12, 3469–3488, 10.5194/bg-12-3469-2015, 2015.

755 Schuur, E. A. G., McGuire, A. D., Schädel, C., Grosse, G., Harden, J. W., Hayes, D. J., Hugelius, G., Koven, C. D., Kuhry,
756 P., Lawrence, D. M., Natali, S. M., Olefeldt, D., Romanovsky, V. E., Schaefer, K., Turetsky, M. R., Treat, C. C., and
757 Vonk, J. E.: Climate change and the permafrost carbon feedback, *Nature*, 520, 171–179, 10.1038/nature14338, 2015.

758 Sheffield, J., Barrett, A., Colle, B., Fernando, D., Fu, R., Geil, K., Hu, Q., Kinter, J., Kumar, S., Langenbrunner, B.,
759 Lombardo, K., Long, L., Maloney, E., Mariotti, A., Meyerson, J., Mo, K., Neelin, J., Nigam, S., Pan, Z., and Yin, L.:
760 North American Climate in CMIP5 Experiments. Part I: Evaluation of Historical Simulations of Continental and
761 Regional Climatology*, *Journal of Climate*, 26, 9209–9245, 10.1175/JCLI-D-12-00592.1, 2013.

762 Smith, S. L., O’Neill, H. B., Isaksen, K., Noetzli, J., and Romanovsky, V. E.: The changing thermal state of permafrost,
763 *Nature Reviews Earth & Environment*, 3, 10–23, 10.1038/s43017-021-00240-1, 2022.

764 Spahni, R., Joos, F., Stocker, B. D., Steinacher, M., and Yu, Z. C.: Transient simulations of the carbon and nitrogen
765 dynamics in northern peatlands: from the Last Glacial Maximum to the 21st century, *Clim. Past*, 9, 1287–1308,
766 10.5194/cp-9-1287-2013, 2013.

767 Stocker, B. D., Spahni, R., and Joos, F.: DYPTOP: a cost-efficient TOPMODEL implementation to simulate sub-grid spatio-
768 temporal dynamics of global wetlands and peatlands, *Geosci. Model Dev.*, 7, 3089–3110, 10.5194/gmd-7-3089-2014,
769 2014.

770 Tang, R., He, B., Chen, H. W., Chen, D., Chen, Y., Fu, Y. H., Yuan, W., Li, B., Li, Z., Guo, L., Hao, X., Sun, L., Liu, H.,
771 Sun, C., and Yang, Y.: Increasing terrestrial ecosystem carbon release in response to autumn cooling and warming,
772 *Nature Climate Change*, 12, 380–385, 10.1038/s41558-022-01304-w, 2022.

773 Tape, K. E. N., Sturm, M., and Racine, C.: The evidence for shrub expansion in Northern Alaska and the Pan-Arctic, *Global*
774 *Change Biology*, 12, 686–702, <https://doi.org/10.1111/j.1365-2486.2006.01128.x>, 2006.

- 775 Treat, C. C., Jones, M. C., Brosius, L., Grosse, G., Walter Anthony, K., and Frolking, S.: The role of wetland expansion and
776 successional processes in methane emissions from northern wetlands during the Holocene, *Quaternary Science Reviews*,
777 257, 106864, <https://doi.org/10.1016/j.quascirev.2021.106864>, 2021.
- 778 Turunen, J., Tomppo, E., Tolonen, K., and Reinikainen, A.: Estimating carbon accumulation rates of undrained mires in
779 Finland—application to boreal and subarctic regions, *The Holocene*, 12, 69-80, 10.1191/0959683602h1522rp, 2002.
- 780 Wood, E. F., Lettenmaier, D. P., and Zartarian, V. G.: A land-surface hydrology parameterization with subgrid variability for
781 general circulation models, *Journal of Geophysical Research: Atmospheres*, 97, 2717-2728,
782 <https://doi.org/10.1029/91JD01786>, 1992.
- 783 Xu, J., Morris, P. J., Liu, J., and Holden, J.: PEATMAP: Refining estimates of global peatland distribution based on a meta-
784 analysis, *CATENA*, 160, 134-140, <https://doi.org/10.1016/j.catena.2017.09.010>, 2018.
- 785 Yi, Y. and Kimball, J. S.: ABoVE: Active Layer Thickness from Remote Sensing Permafrost Model, Alaska, 2001-2015,
786 10.3334/ORNLDAAC/1760, 2020.
- 787 Yokohata, T., Saito, K., Ito, A., Ohno, H., Tanaka, K., Hajima, T., and Iwahana, G.: Future projection of greenhouse gas
788 emissions due to permafrost degradation using a simple numerical scheme with a global land surface model, *Progress in*
789 *Earth and Planetary Science*, 7, 56, 10.1186/s40645-020-00366-8, 2020.
- 790 Yu, Z., Beilman, D., and Jones, M.: Sensitivity of Northern Peatland Carbon Dynamics to Holocene Climate Change,
791 Washington DC American Geophysical Union Geophysical Monograph Series, 184, 55-69, 10.1029/2008GM000822,
792 2009.
- 793 [Zhao, B., Zhuang, Q., and Frolking, S.: Modeling Carbon Accumulation and Permafrost Dynamics of Northern Peatlands
794 Since the Holocene, *Journal of Geophysical Research: Biogeosciences*, 127, e2022JG007009,
795 <https://doi.org/10.1029/2022JG007009>, 2022b. Zhao, B., Zhuang, Q., and Frolking, S.: Modeling carbon accumulation
796 and greenhouse gas emissions of northern peatlands since the Holocene \(in review\), 2022a.](https://doi.org/10.1029/2022JG007009)
- 797 Zhao, B., Zhuang, Q., Treat, C., and Frolking, S.: A Model Intercomparison Analysis for Controls on C Accumulation in
798 North American Peatlands, *Journal of Geophysical Research: Biogeosciences*, 127, e2021JG006762,
799 <https://doi.org/10.1029/2021JG006762>, 2022ab.
- 800 Zhao, R. J., Liu, X. R., and Singh, V. P.: The Xinanjiang model,
- 801 Zhuang, Q., McGuire, A. D., O'Neill, K. P., Harden, J. W., Romanovsky, V. E., and Yarie, J.: Modeling soil thermal and
802 carbon dynamics of a fire chronosequence in interior Alaska, *Journal of Geophysical Research: Atmospheres*, 107, FFR
803 3-1-FFR 3-26, <https://doi.org/10.1029/2001JD001244>, 2002.
- 804 Zhuang, Q., Melillo, J. M., Kicklighter, D. W., Prinn, R. G., McGuire, A. D., Steudler, P. A., Felzer, B. S., and Hu, S.:
805 Methane fluxes between terrestrial ecosystems and the atmosphere at northern high latitudes during the past century: A
806 retrospective analysis with a process-based biogeochemistry model, *Global Biogeochemical Cycles*, 18,
807 <https://doi.org/10.1029/2004GB002239>, 2004.
- 808 Zomer, R. J. and Trabucco, A.: Version 3 of the “Global Aridity Index and Potential Evapotranspiration (ET0) Database”:
809 Estimation of Penman-Monteith Reference Evapotranspiration. (In Press). [dataset],
810 <https://cgiarcsi.community/2019/01/24/globalaridity-index-and-potential-evapotranspiration-climate-database-v3/>, 2022.

811

812 Supplemental References

- 813 Hugelius, G., Loisel, J., Chadburn, S., Jackson, R. B., Jones, M., MacDonald, G., Marushchak, M., Olefeldt, D., Packalen,
814 M., Siewert, M. B., Treat, C., Turetsky, M., Voigt, C., and Yu, Z.: Large stocks of peatland carbon and nitrogen are
815 vulnerable to permafrost thaw, *Proceedings of the National Academy of Sciences*, 117, 20438-
816 10.1073/pnas.1916387117, 2020.
- 817 Melton, J. R., Chan, E., Millard, K., Fortier, M., Winton, R. S., Martín-López, J. M., Cadillo-Quiroz, H., Kidd, D., and
818 Verchot, L. V.: A map of global peatland extent created using machine learning (Peat-ML), *Geosci. Model Dev.*
819 *Discuss.*, 2022, 1-44, 10.5194/gmd-2021-426, 2022.
- 820 Obu, J., Westermann, S., Barboux, C., Bartsch, A., Delaloye, R., Grosse, G., Heim, B., Hugelius, G., Irrgang, A., Käib, A.
821 M., Krosileitner, C., Matthes, H., Nitze, I., Pellet, C., Seifert, F. M., Strozzi, T., Wegmüller, U., Wieczorek, M., and
822 Wiesmann, A.: ESA Permafrost Climate Change Initiative (Permafrost_cci): Permafrost Climate Research Data

823 Package v1., Centre for Environmental Data Analysis [dataset],
824 <https://catalogue.ceda.ac.uk/uuid/1f88068e86304b0fbd34456115b6606f>, 2020.

825 ~~Xu, J., Morris, P. J., Liu, J., and Holden, J.: PEATMAP: Refining estimates of global peatland distribution based on a meta-~~
826 ~~analysis, CATENA, 160, 134–140, <https://doi.org/10.1016/j.catena.2017.09.010>, 2018.~~

827 Yi, Y. and Kimball, J. S.: ABoVE: Active Layer Thickness from Remote Sensing Permafrost Model, Alaska, 2001–2015,
828 10.3334/ORNLDAAC/1760, 2020.

829 ~~Zhao, B., Zhuang, Q., and Frolking, S.: Modeling Carbon Accumulation and Permafrost Dynamics of Northern Peatlands~~
830 ~~Since the Holocene, Journal of Geophysical Research: Biogeosciences, 127, e2022JG007009,~~
831 ~~<https://doi.org/10.1029/2022JG007009>, 2022b. Zhao, B., Zhuang, Q., and Frolking, S.: Modeling carbon accumulation~~
832 ~~and greenhouse gas emissions of northern peatlands since the Holocene (in review), 2022.~~

833 Zomer, R. J. and Trabucco, A.: Version 3 of the “Global Aridity Index and Potential Evapotranspiration (ET0) Database”:
834 Estimation of Penman-Monteith Reference Evapotranspiration. (In Press). [dataset],
835 <https://cgiarcsi.community/2019/01/24/globalaridity-index-and-potential-evapotranspiration-climate-database-v3/>, 2022.

836